iScience

CellPress
OPEN ACCESS

Article

Myoneurin regulates BMP signaling by competing with Ppm1a for Smad binding

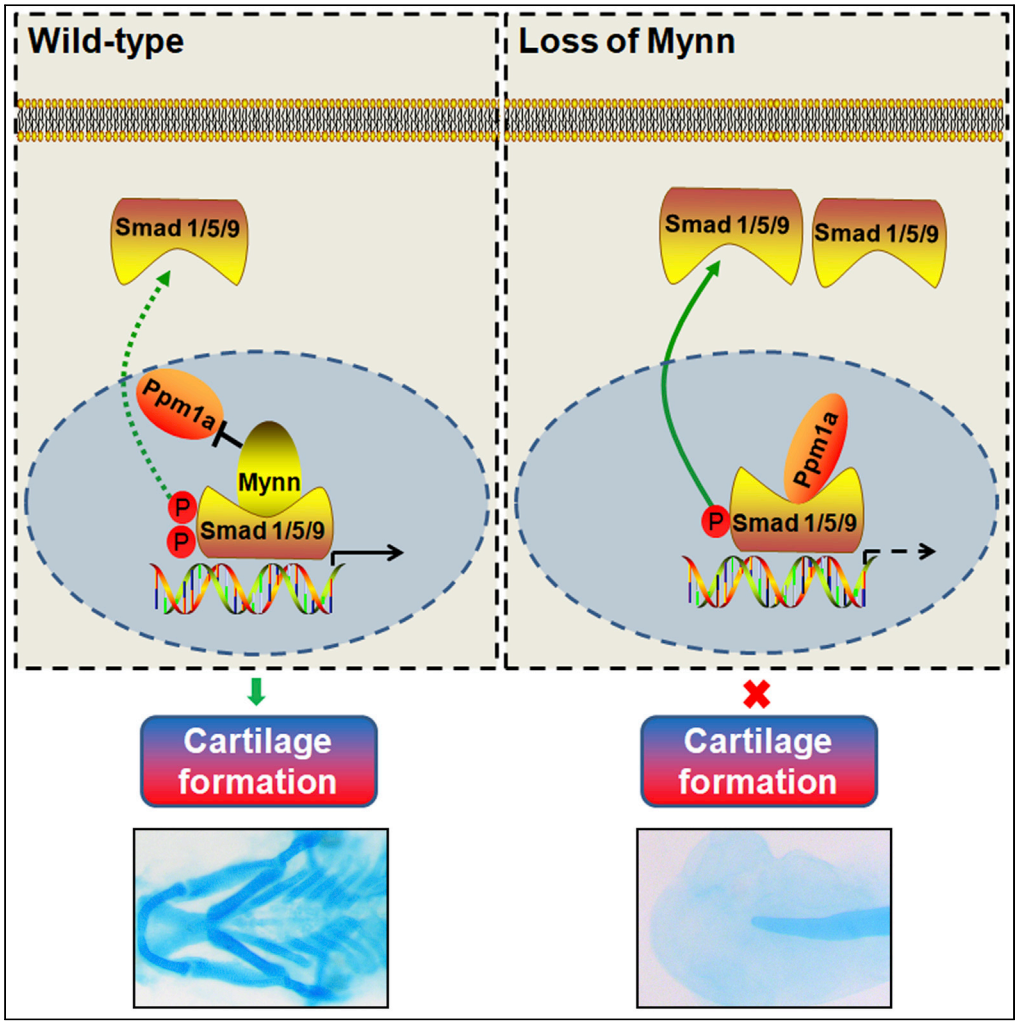

Shuyan Yang, Guozhu Ning, Yiming Hou, ..., Jianxin Wu, Ting Zhang, Qiang Wang

jianxinwu_2000@163.com (J.W.)
Zhangtingcv@126.com (T.Z.)
qiangwang@scut.edu.cn (Q.W.)

Highlights

mynn gene is essential for pharyngeal cartilage development

mynn is required for the proliferation, differentiation, and survival of the CNCCs

Mynn has an evolutionarily conserved function in supporting BMP signal

Mynn maintains BMP signal activity by competing with Ppm1a for Smad binding

Yang et al., iScience *25*, 104495
June 17, 2022
https://doi.org/10.1016/j.isci.2022.104495

iScience

CellPress
OPEN ACCESS

Article

Myoneurin regulates BMP signaling by competing with Ppm1a for Smad binding

Shuyan Yang,[1,5] Guozhu Ning,[2,3,5] Yiming Hou,[3] Yu Cao,[3] Jin Xu,[2] Jianxin Wu,[4,*] Ting Zhang,[1,*] and Qiang Wang[2,3,6,*]

SUMMARY

A delicate balance of BMP activity is critical for tissue formation and organogenesis. However, the mechanical molecular details in ensuring the proper duration and intensity of BMP signaling have yet to be fully elucidated. Here, we identified a zebrafish mutant with a disrupted gene encoding for the BTB/POZ and zinc finger protein myoneurin (Mynn). *mynn*$^{-/-}$ mutants exhibited severe loss of pharyngeal cartilage elements, owing to poor proliferation, blocked differentiation, and low viability of cranial neural crest cells. Depletion of *mynn* in both zebrafish embryos and mammalian cells led to a reduction of the BMP signal activity. Mechanistically, Mynn interacts with Smad proteins in the nucleus, thereby disrupting the association between Smad protein and the phosphatase Ppm1a. Ultimately, this interaction prevents Smad dephosphorylation. More broadly, our findings may provide a new strategy to balance BMP signal activity via competitive binding of Mynn and Ppm1a to Smad proteins during pharyngeal cartilage formation.

INTRODUCTION

Craniofacial malformations are common congenital birth defects that impact the development of the head, face, and neck. Globally, they account for approximately three-fourths of all human birth defects (Cordero et al., 2011). Aberrant cartilage development is one of the primary causes of craniofacial anomalies (Hamerman, 1989). The neurocranium, which is composed of both the upper and front portions of the skull, arises from both the cranial neural crest cells (CNCCs) and mesoderm. Comparatively, the pharyngeal skeleton—which includes the jaw and branchial arches—is derived exclusively from CNCCs (Yelick and Schilling, 2002). CNCCs originate from the boundary between the epidermal and neural territories during the process of neurulation. Subsequently, these cells undergo an epithelial-to-mesenchymal transition, after which they collectively migrate from the midbrain and hindbrain to pharyngeal arches (Donoghue et al., 2008; Trainor and Nieto, 2003). Once they have reached their destinations, the CNCCs proliferate and differentiate into chondrocytes, which produce a large amount of extracellular matrix consisting of type II collagen (Col2) (Hall and Miyake, 1995).

These dynamic processes that occur during pharyngeal cartilage development are controlled by a diverse set of interacting signals such as BMP, Wnt, and FGF pathways (Crump et al., 2004; LaBonne and Bronner-Fraser, 1999; Nie et al., 2006). In particular, previous studies have demonstrated that BMP signaling is essential for the induction and proper migration of CNCCs to facial primordia (Kanzler et al., 2000; Liem et al., 1995; Tribulo et al., 2003; Wilson et al., 1997). Recent reports from our laboratory have provided evidence that balanced BMP signaling is achieved by the interaction between BMP ligands and their antagonist Noggin3. Moreover, this balanced interaction is necessary to ensure proper proliferation, differentiation, and survival of postmigratory CNCCs (Li et al., 2018; Ning et al., 2013). However, further studies are needed to identify additional genes involved in controlling the delicate balance of BMP signaling during cartilage development.

The BTB/POZ and zinc finger (BTB/POZ-ZF) protein family is classified according to the presence of an N-terminal POZ domain and a C-terminal C2H2 ZF motif. This family comprises a diverse group of transcription factors that either activate or suppress the transcription of distinct genes (Kelly and Daniel, 2006). Various vertebrate POZ-ZF proteins have been isolated and characterized; many are linked either directly or indirectly to human cancers (e.g. B cell lymphoma 6 (Bcl-6), promyelocytic leukemia zinc finger (PLZF),

[1]Beijing Municipal Key Laboratory of Child Development and Nutriomics, Capital Institute of Pediatrics, Beijing 100020, China

[2]Division of Cell, Developmental and Integrative Biology, School of Medicine, South China University of Technology, Guangzhou 510006, China

[3]State Key Laboratory of Membrane Biology, Institute of Zoology, University of Chinese Academy of Sciences, Chinese Academy of Sciences, Beijing, China

[4]Beijing TongRen Hospital, Capital Medical University, 17 Hougou Street, Chong Wen Men, Beijing 100005, PR China

[5]These authors contributed equally

[6]Lead contact

*Correspondence: jianxinwu_2000@163.com (J.W.), Zhangtingcv@126.com (T.Z.), qiangwang@scut.edu.cn (Q.W.)

https://doi.org/10.1016/j.isci.2022.104495

and hypermethylated in cancer 1 (HIC-1)) (Chen et al., 1993, 2003; Kelly and Daniel, 2006; McConnell et al., 2003; Wales et al., 1995). These structurally related proteins have also been implicated in the control of a wide range of developmental events in various invertebrates and vertebrates (Barna et al., 2000; Kelly and Daniel, 2006; Kim et al., 2004; Kojima et al., 2001; Xiong and Montell, 1993). Previous studies have suggested that the POZ domain of this family functions as a conserved protein-protein interaction motif to recruit a number of epigenetic regulators, including HDACs, mSin3a, SMRT, and NCoR. These regulators then modulate the expression of a variety of target genes (Bardwell and Treisman, 1994; Chauchereau et al., 2004; Dhordain et al., 1998). Interestingly, the POZ-ZF family members Kaiso and HIC-1 antagonize Wnt signaling by interacting with TCF proteins during both embryonic development and carcinogenesis (Chauchereau et al., 2004; Park et al., 2005). However, whether POZ-ZF proteins associate with the cellular effectors of other signaling pathways remains to be explored.

Myoneurin (*Mynn* gene) encodes for a protein with features of a BTB/POZ-ZF protein and was initially cloned during a screening of the human λgt11 testicular library (Alliel et al., 2000). Murine Mynn protein is highly homologous to its human ortholog. Moreover, *Mynn* transcripts have been identified in both mouse embryos and adult tissues, including cerebellum, skeletal muscle, neuromuscular system, testis, heart, brain, and liver (Alliel et al., 2000; Cifuentes-Diaz et al., 2004). Because its expression is strongly elevated through increased gene copy, *Mynn* has been identified as one of the potential drivers in ovarian cancer (Ramakrishna et al., 2010). Moreover, genotyping analysis in patients diagnosed with bladder cancer revealed a strong cumulative association between a single nucleotide polymorphism in *Mynn* and tumorigenesis (Polat et al., 2019). Collectively, these observations suggest a potential role for *Mynn* throughout development and adulthood. Despite this, the developmental and physiological roles of *Mynn* have been largely unknown and unexplored.

In this study, we identified a zebrafish *mynn* mutant line using a *Tol2* transposon-mediated gene trapping approach. Homozygous *mynn* mutant embryos showed multiple developmental defects, including pericardial edema, smaller heads and eyes, curved tails, rough skins, and a near-complete loss of the pharyngeal cartilages. In particular, the cartilage defects are resulted from impaired proliferation, differentiation, and maintenance of CNCCs. We found that the depletion of *mynn* in embryos and mammalian cells led to a significant decrease in BMP signaling, which partially account for the observed defects in cartilage development. Moreover, biochemical and functional studies revealed that Mynn interacts with Smad proteins. Importantly, this interaction disrupts their association with Ppm1a, which is a serine/threonine phosphatase. This disruption then supports the phosphorylation status of Smad proteins. Hence, these findings uncovered an unexpected role for Mynn in balancing BMP signal activity through competitive binding to Smad proteins with Ppm1a during pharyngeal cartilage development.

RESULTS

T054 mutants possess a marked defect in pharyngeal cartilage formation

To identify the genes essential for zebrafish embryo development, an insertional mutagenesis screen with a Tol2 transposon-mediated gene trap strategy was used. This approach allowed for the isolation of mutants with various developmental defects in specific tissues and organs (Han et al., 2011; Zhao et al., 2008). The Tol2 transposon-based trap vector TSG contained a promoter-less EGFP reporter, with fish carrying TSG insertions showing specific GFP expression patterns under the control of neighboring endogenous promoters (Zhao et al., 2008). One of the trapped lines, T054, was notable as a proportion of the embryos from heterozygous F1 intercrosses exhibited multiple morphological defects, including pericardial edema, smaller heads and eyes, curved tails, rough skins, and severe jaw malformations from 48 to 96 h postfertilization (hpf) (Figure 1A). Such embryos died by approximately 120 hpf. During T054 embryo development, the expression of EGFP was clearly observed at the one-cell stage, suggesting its maternal origin (Figure S1). Then, EGFP was ubiquitously expressed until 24 hpf, becoming more prominent in the head, lens, otic vesicle, and trunk musculature during the pharyngula period (Figure S1). From 48 to 72 hpf, intensive EGFP was detected in the developing pharyngeal arches (Figure 1B). Under close observation of the pharyngeal region at higher magnification, the pharyngeal cartilages were clearly EGFP-positive (Figure 1B). Moreover, immunostaining experiments showed that in T054 embryos at 72 hpf, the EGFP-positive chondrocytes located in the pharyngeal arches had high levels of the secreted primary cartilage matrix protein Col2 (Figure 1C). Taken together, these results suggest that the gene trapped by Tol2 transposon in the T054 line is expressed in the pharyngeal arches. Critically, the interruption of this locus may be responsible for the observed mutant phenotype.

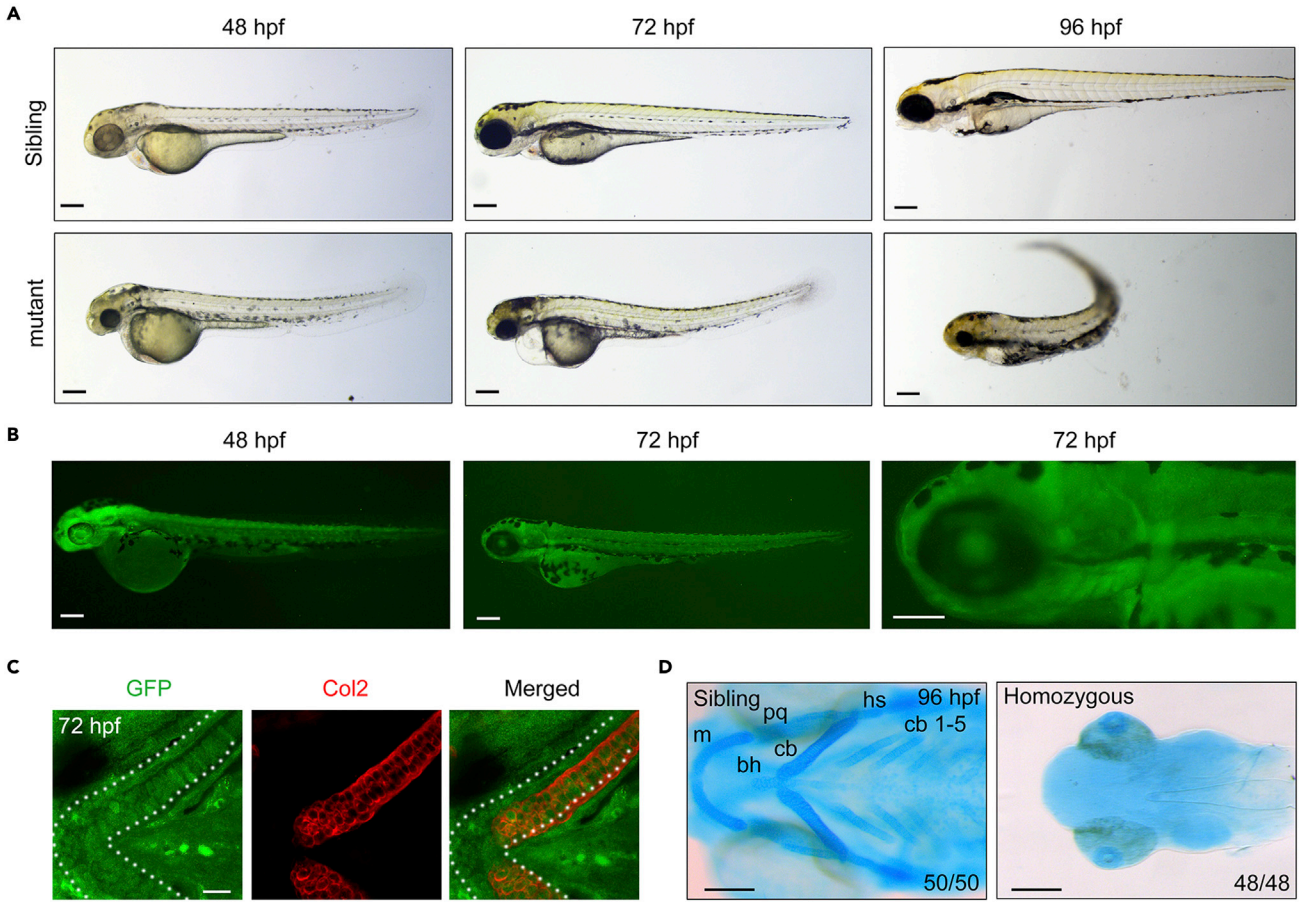

Figure 1. The GFP expression and developmental defects in T054 embryos

(A) Morphology of T054 mutants at indicated stages. Note that mutant embryos had a darker head, rough skin, reduced size of head and eyes, severe craniofacial jaw malformations, and curly posterior trunk with stage-dependent degrees. Scale bars, 200 μm.

(B) Fluorescent images of T054 embryos. The pictured embryos were heterozygotes. Scale bars, 200 μm.

(C) Immunostaining of chondrocytes by anti-Col2 and GFP antibody. T054 heterozygous embryos at 72 hpf were co-immunostained with anti-Col2 (red) and anti-GFP (green) antibodies. Scale bar, 20 μm.

(D) Craniofacial cartilages stained with Alcian blue. Note that almost no cartilages could be seen in the T054 mutant embryos. The cartilages were positioned with anterior to the left, and ceratobranchial (cb), ceratohyal (ch), Meckel's cartilage (m), palatoquadrate (pq), and hyosymplectic (hs) cartilages were shown. Scale bars, 200 μm.

Interestingly, the offspring of T054 heterozygous fish showed a different expression intensity of the EGFP reporter. In agreement with Mendel's law of segregation, among the 2095 embryos at 24 hpf from 23 pairwise crosses of heterozygous fish, 24% produced strong EGFP expression (homozygous insertion), 51% expressed moderate EGFP (heterozygous insertion), and 25% were negative for EGFP. Heterozygous fish were mated with wild-type fish to generate F2 families. We observed an identical EGFP expression pattern in approximately 50% of their progeny. Simultaneously, no EGFP expression was detected in the other half, implying that a single locus has been trapped in the T054 embryos. The F2 embryos that had GFP expression exhibited normal morphological features and survived to adulthood. Consistently, Alcian blue staining results revealed that, in comparison to wild-type and heterozygous siblings, T054 homozygous mutants derived from F2 fish lost almost all their pharyngeal skeletal elements (Figure 1D). In addition, the dorsal neurocrania were also absent in the homozygous mutants (Figure 1D). Collectively, these data indicate that the insertion of Tol2 element in the T054 embryos causes an inherited disorder associated with severe defects in the craniofacial skeleton.

The interrupted gene in the T054 line is *mynn*

To identify the trapped gene in the T054 line, we performed 5′-RACE and thermal asymmetric interlaced PCR (TAIL-PCR). Sequence and bioinformatic analyses revealed that the Tol2 transposon inserted into

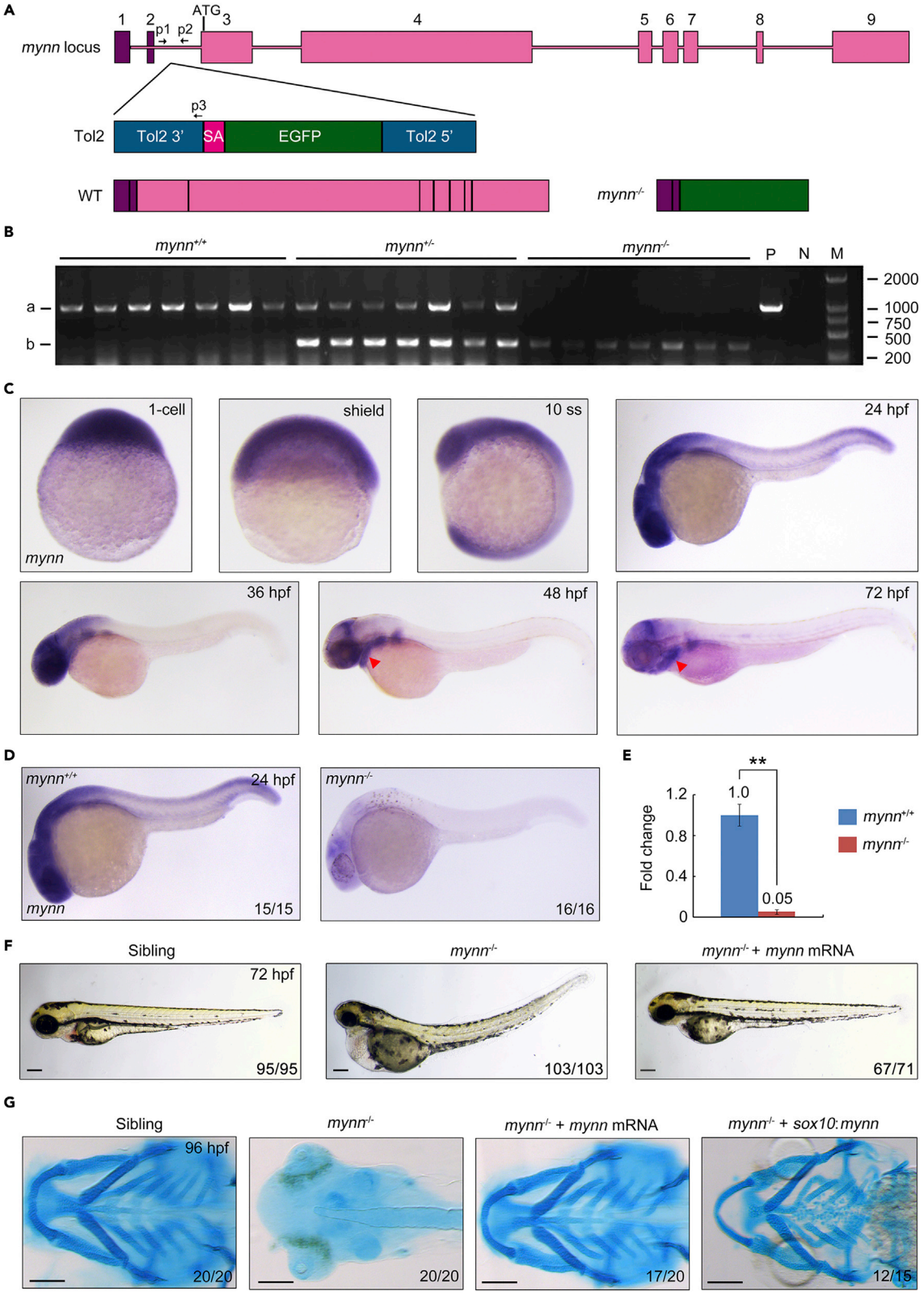
A
mynn locus
1
2
p1
p2
ATG
3
4
5
6
7
8
9
p3
Tol2
Tol2 3'
SA
EGFP
Tol2 5'
WT
mynn-/-
B
mynn+/+
mynn+/-
mynn-/-
P
N
M
a
b
2000
1000
750
500
200
C
1-cell
mynn
shield
10 ss
24 hpf
36 hpf
48 hpf
72 hpf
D
mynn+/+
24 hpf
mynn
15/15
mynn-/-
16/16
E
**
1.2
0.8
0.4
0
Fold change
1.0
0.05
mynn+/+
mynn-/-
F
Sibling
72 hpf
95/95
mynn-/-
103/103
mynn-/- + mynn mRNA
67/71
G
Sibling
96 hpf
20/20
mynn-/-
20/20
mynn-/- + mynn mRNA
17/20
mynn-/- + sox10:mynn
12/15

Figure 2. *mynn* was trapped in the T054 line

(A) Genomic structure of the *mynn* locus and putative transcripts. Exons are numbered. The binding positions and directions of the primers used in (B) are indicated. Note that in the homozygous embryos, the transcripts of *mynn* only contain the first two exons at the upstream of the translational initiation site.

(B) Genotyping of individual embryos by PCR. Embryos collected from *mynn* heterozygote intercrosses were separated based on GFP intensity. Three primers, p1, p2, and p3, were used together for PCR. The upper (a) and lower (b) bands represented the wild-type and recombinant allele, respectively. M, molecular marker; P, positive control; N, negative control with no template.

(C) Expression pattern of *mynn* in wild-type embryos at indicated stages detected by *in situ* hybridization. The transcripts are overt in the pharyngeal region at 48 and 72 hpf as indicated by red arrowheads.

(D) Expression pattern of *mynn* in embryos from different genotypes. Note that the *mynn* expression in $mynn^{-/-}$ embryos was almost disappeared.

(E) RT-PCR analysis of *mynn* transcripts in wild-type and mutant embryos at 24 hpf. β-actin was used as an internal control. The data were presented as mean ± SD from three independent biological repeats. Total RNA of each group was extracted from a pool of 30 embryos. **, $p < 0.01$ (by Student's *t* test).

(F) Overexpression of *mynn* rescued the mutant phenotype. *mynn* heterozygote intercrosses were injected with 200 pg *mynn* mRNA at the one-cell stage. The homozygous mutants were sorted out at 24 hpf by their EGFP intensity, and their morphology was observed at 72 hpf. The ratio of embryos with presented morphology was indicated. Scale bars, 200 μm.

(G) Head skeletons stained with Alcian blue. Note that cartilages of $mynn^{-/-}$ mutants were missed and the missing cartilages could be rescued by injection of 200 pg *mynn* mRNA into $mynn^{-/-}$ embryos at the one-cell stage or specific overexpression of *mynn* in $sox10^{+}$ NCCs. Scale bars, 200 μm.

the second intron of the *mynn* gene (Figure 2A). We then confirmed the presence of the Tol2 element in *mynn* homozygotes and heterozygotes by PCR-based genotyping assay with specific primers (Figures 2A and 2B). Subsequently, we investigated the spatiotemporal expression of *mynn* by whole-mount *in situ* hybridization (WISH) using an antisense probe against the 3′ end of the *mynn* transcript. Similar to the expression of the EGFP reporter in T054 mutants, *mynn* transcripts were detected in one-cell stage embryos and distributed ubiquitously until 24 hpf. By 24 hpf, *mynn* transcripts were enriched in the central nervous system. From 48 to 72 hpf, *mynn* expression was evident in the midbrain-hindbrain boundary, pectoral fin, and pharyngeal arches (Figure 2C).

The zebrafish *mynn* locus consists of 9 exons and 8 introns and has an open reading frame of 2610 base pairs, which encodes a putative peptide of 808 amino acids (Figure 2A). Since the putative translation start codon of *mynn* was located in the third exon (Figure 2A), we speculated that the expression of the coding sequence and 3′ untranslated region protein of the *mynn* gene would be disrupted by the transposon inserted in the mutant line. In support of our hypothesis, we found that the expression of *mynn* in $mynn^{-/-}$ mutants was either dramatically reduced (Figures 2D and 2E). Moreover, microinjection of an antisense *mynn* morpholino (*mynn* MO), which efficiently repressed the translation of *mynn-EGFP* transcripts, resulted in morphological malformations and cartilage phenotypes mimicking the ones observed in $mynn^{-/-}$ mutants (Figures S2A–S2C). Therefore, these results demonstrate that *mynn* is the interrupted gene in the T054 line.

Endodermal pouches play important roles in patterning the pharyngeal arches, which occurs through tissue-tissue interactions (Couly et al., 2002; David et al., 2002; Knight and Schilling, 2006; Li et al., 2018; Ruhin et al., 2003). Zn5 labels for the pouch endoderm in zebrafish embryos (Schwend and Ahlgren, 2009). Immunostaining with a Zn5 antibody revealed that the pouches formed normally in $mynn^{-/-}$ mutants (Figure S2D), suggesting that the loss of pharyngeal cartilages in $mynn^{-/-}$ mutants is not due to pouch defects.

To further confirm that the loss of pharyngeal skeleton in $mynn^{-/-}$ mutants is a direct result of *mynn* deficiency, we examined whether injection of *mynn* mRNA could rescue the mutant phenotype. As expected, the morphological malformations and cartilage defects were successfully rescued after injection of 200 pg of *mynn* mRNA into one-cell stage $mynn^{-/-}$ embryos (Figures 2F and 2G). Moreover, overexpression of *mynn* under the control of *sox10* promoter, which is well known to drive a tissue-specific expression in the cranial and trunk neural crest cells (NCCs) (Carney et al., 2006), significantly reduced the cartilage loss in $mynn^{-/-}$ mutants (Figure 2G), indicating a cell-autonomous role for *mynn* in head skeleton development. Interestingly, most morphological defects in $mynn^{-/-}$ mutants, including smaller heads and eyes, rough skin, and curved tails, were also alleviated by such tissue-specific expression of *mynn* (Figure S3), further implying a non-cell-autonomous function of NCC-expressed *mynn* during embryogenesis.

Taken together, the above data provide strong evidence that we identified a functional transposon insertion in *mynn* gene, which is essential for the development of pharyngeal cartilage in zebrafish.

Loss of *mynn* compromises the proliferation and chondrogenic differentiation of CNCCs

The formation of pharyngeal skeletons involves multiple steps, including specification of CNCCs, migration of CNCCs ventrally into the pharyngeal arches, prechondrogenic condensation, and chondrogenic

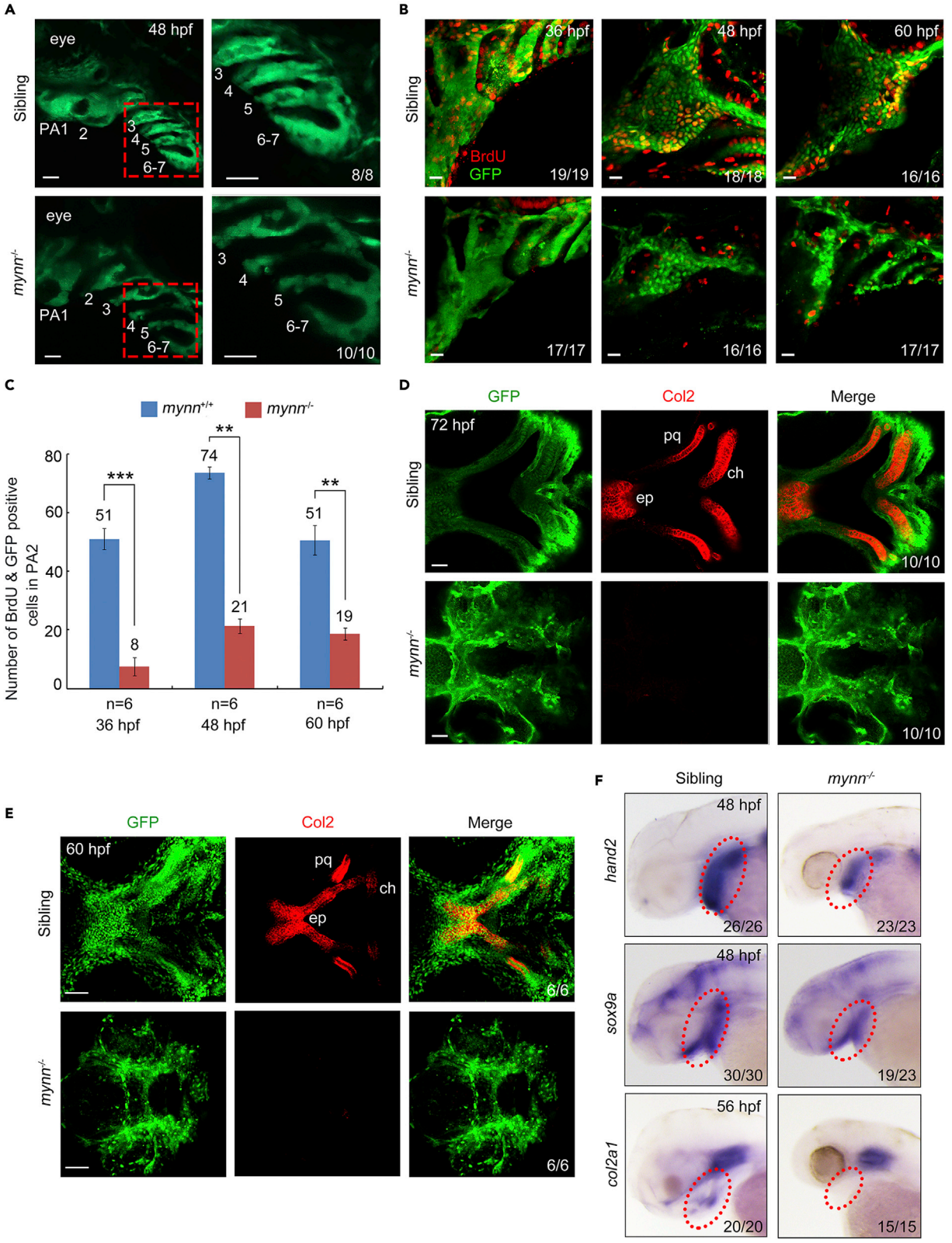
A
Sibling
mynn-/-
eye
48 hpf
PA1
2
3
4
5
6-7
8/8
10/10
B
36 hpf
48 hpf
60 hpf
BrdU
GFP
19/19
18/18
16/16
17/17
16/16
17/17
C
mynn+/+
mynn-/-
Number of BrdU & GFP positive cells in PA2
***
**
**
51
8
74
21
51
19
n=6
36 hpf
n=6
48 hpf
n=6
60 hpf
D
GFP
Col2
Merge
72 hpf
pq
ch
ep
10/10
10/10
E
60 hpf
6/6
6/6
F
Sibling
mynn-/-
hand2
sox9a
col2a1
48 hpf
56 hpf
26/26
23/23
30/30
19/23
20/20
15/15

Figure 3. Reduced cell proliferation and differentiation of CNCCs in *mynn*$^{-/-}$ embryos

(A) Live imaging of the pharyngeal region of *mynn*$^{-/-}$ embryos in *Tg(fli1:EGFP)* background. The pharyngeal arches were numbered. The boxed areas in the left pannel were enlarged in the right panels. PA: pharyngeal arch. Scale bars, 20 μm.

(B and C) BrdU incorporation experiments showed reduced proliferating CNCCs in *mynn*$^{-/-}$ mutants. BrdU-treated *mynn*$^{-/-}$ mutants with *fli1:EGFP* expression were harvested at indicated stages and stained with anti-BrdU (red) and anti-GFP (green) antibodies. The pharyngeal regions were observed by confocal microscopy (B). Scale bars, 20 μm. The number of BrdU^{+} and GFP^{+} cells in the second pharyngeal arch was calculated from six embryos (C). Error bars indicate ±S.D. **, $p < 0.01$; ***, $p < 0.001$ (by Student's *t* test).

(D and E) Detection of Col2 proteins in the pharyngeal arches. Wild-type and *mynn*$^{-/-}$ embryos in *Tg(fli1:EGFP)* background at 60 (E) or 72 (D) hpf were co-immunostained with anti-GFP (green) and anti-Col2 (red) antibodies. The palatoquadrate (pq), ethmoid plate (ep), and ceratohyal (ch) cartilages were shown with anterior to the left. Scale bars, in panel D, 20 μm; in panel E, 50 μm.

(F) Expression pattern of *hand2*, *sox9a*, and *col2a1* in *mynn*$^{-/-}$ embryos and their siblings at indicated stages detected by *in situ* hybridization.

differentiation (Ning et al., 2013; Zheng et al., 2012). To precisely dissect the role of *mynn* in pharyngeal cartilage development at the cellular level, the expression of several markers was first examined in *mynn*$^{-/-}$ mutants. We found that the *mynn*$^{-/-}$ embryos showed indistinguishable expression patterns of the early neural crest specification marker *foxd3* at 11 hpf when compared with their wild-type and heterozygous counterparts (Figure S4), suggesting a normal induction of CNCCs. Moreover, CNCC migration was not noticeably disturbed by *mynn* depletion as the expression of postmigratory markers *dlx2* and *sox9a* in *mynn*$^{-/-}$ mutants was comparable to that in control animals at 18 and 24 hpf (Figure S4).

To uncover the cellular defects responsible for the reduction of pharyngeal cartilage induced by *mynn* inactivation, *in vivo* imaging was performed on *Tg(fli1:EGFP)* embryos, which expresses EGFP in CNCC derivatives (Lawson and Weinstein, 2002; McGurk et al., 2014). We observed that, in *mynn*$^{-/-}$ mutants at 48 hpf, the EGFP-positive CNCCs aggregated as prechondrogenic condensations. However, these condensations became much smaller (Figure 3A), suggesting that the loss of cartilage in *mynn*$^{-/-}$ mutants may be due to proliferation defects of CNCCs. To test this hypothesis, we performed bromodeoxyuridine (BrdU) incorporation assays in *mynn*$^{-/-}$ mutants and their siblings at 36, 48, and 60 hpf. We found that the BrdU signal was not obviously changed in the trunk region of *mynn*$^{-/-}$ mutants, but distinctly reduced in the eye, brain, and pharynx, where *mynn* was highly expressed (Figure S5A), suggesting a reduction of proliferating cells in multiple head tissues. To further determine whether the proliferation of CNCCs was affected upon *mynn*-depletion, BrdU incorporation experiments were performed on embryos with the *Tg(fli1:EGFP)* transgenic reporter. As expected, depletion of *mynn* resulted in a notable elimination of proliferating BrdU^{+} CNCCs (Figures 3B and 3C).

Furthermore, immunostaining analysis indicated that Col2 signal, which was clearly seen in the first arch-derived palatoquadrate (pq) and the second arch-derived ceratohyal (ch) cartilages in control animals at 72 hpf, was almost absent in the arches of *mynn*$^{-/-}$ mutants (Figure 3D). This indicates a failure of chondrogenic differentiation. However, the presence of a large amount of cellular debris in the pharynx of *mynn*$^{-/-}$ mutants raised a possibility that the loss of Col2 might be due to a loss of CNCCs (Figure 3D). To confirm the differentiation defects in the mutants, the expression of Col2 protein was further examined at 60 hpf, when the majority of CNCCs in *mynn*$^{-/-}$ mutant were not broken (Figure 3B). Indeed, there was no detectable expression of Col2 in *mynn*-depleted CNCCs at this developmental stage (Figure 3E). In addition, an apparent diminution in the expression of chondrogenic marker genes, such as *hand2*, *sox9a*, and *col2a1*, was found in *mynn*$^{-/-}$ embryos at 48 or 56 hpf (Figure 3F), demonstrating a crucial role of *mynn* in chondrocyte differentiation.

Collectively, these results explicitly demonstrate that *mynn* is required for the proliferation and chondrogenic differentiation of CNCCs.

mynn is required for the survival of chondrogenic cells

As we have described above, loss of *mynn* impaired the chondrogenic differentiation of CNCCs (Figures 3D and 3E). In siblings, differentiated CNCCs appeared elongated and were organized with a columnar orientation in the arches. Comparatively, no regular chondrocytes and only abundant cellular debris were observed in the pharynx of *mynn*$^{-/-}$ mutants (Figure 3D), suggesting that increased cell death was occurring in these structures.

To confirm this finding, apoptotic analysis using a TUNEL assay was conducted in embryos on the *Tg(fli1:GFP)* transgenic background. Before and at 36 hpf, there were no detectable apoptotic cells in

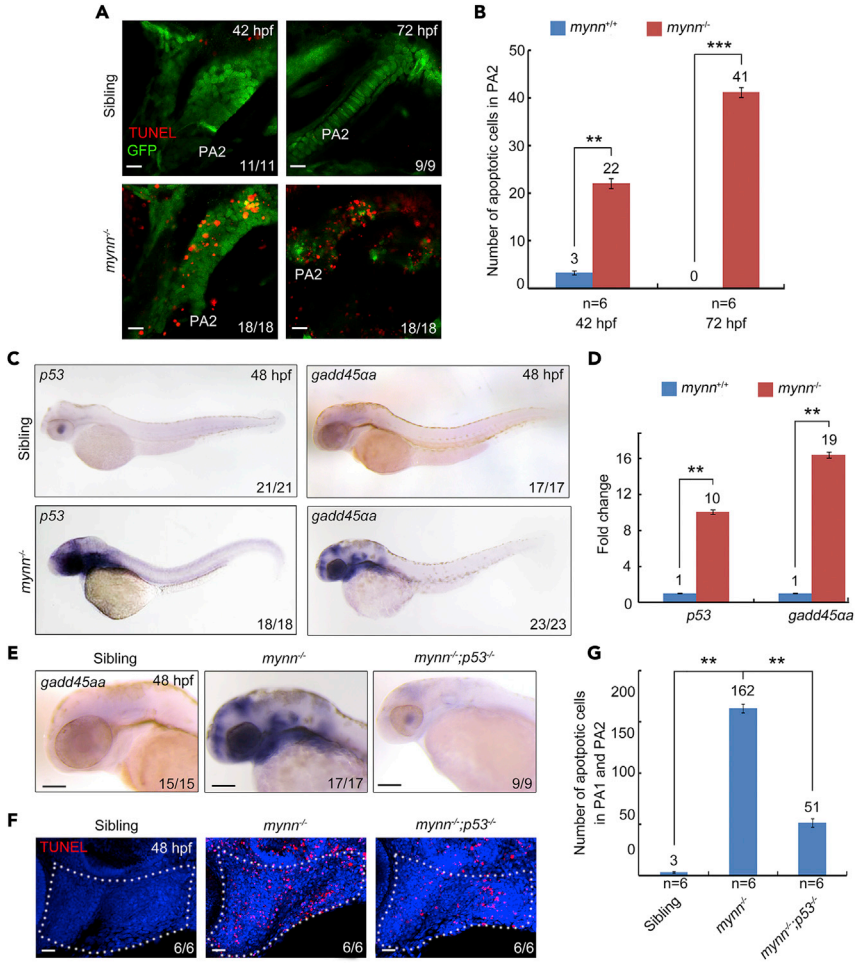

Figure 4. *mynn* mutants exhibit cell death and upregulated p53 signaling

(A and B) Detection of apoptotic cells in the pharyngeal regions. *mynn*-deficient *Tg(fli1:EGFP)* embryos and their siblings were collected at indicated stages for TUNEL assay (A). PA, pharyngeal arch. Scale bars, 10 μm. The number of TUNEL$^+$ and GFP$^+$ cells in PA2 was calculated from six embryos (B). Error bars indicate ±S.D. **, $p < 0.01$; ***, $p < 0.001$ (by Student's *t*-test).

(C) Expression pattern of *p53* and *gadd45αa* in *mynn*$^{-/-}$ embryos at indicated stages.

(D) Real-time PCR analysis of the relative expression level of *p53* and *gadd45αa* in wild-type and *mynn*$^{-/-}$ embryos. β-actin was used as an internal control. Embryos were pre-sorted as mentioned above. The data were presented as mean ± SD from three independent biological repeats. Total RNA of each group was extracted from a pool of 30 embryos. **, $p < 0.01$ (by Student's *t*-test).

(E) Expression analysis of *gadd45αa* by *in situ* hybridization in *mynn*$^{-/-}$ mutants and *mynn*$^{-/-}$;*p53*$^{-/-}$ embryos.

(F and G) The apoptotic cells in the pharyngeal region were clearly decreased in *mynn*$^{-/-}$;*p53*$^{-/-}$ embryos. Indicated embryos were collected at 48 hpf, and then subjected to TUNNEL assays. Representative images were shown in (F). The white dotted lines outline the pharyngeal regions. Scale bars, 20 μm. The number of TUNEL-positive cells in the pharyngeal regions was showed in (G). Error bars indicate ±S.D. **, $p < 0.01$ (by Student's *t*-test).

the pharyngeal region in siblings and *mynn*$^{-/-}$ embryos. However, from 42 to 72 hpf, levels of prechondrogenic and chondrogenic cell apoptosis were significantly elevated in *mynn*$^{-/-}$ mutants when compared with control embryos (Figures 4A and 4B). These results indicate an important role of *mynn* in cell survival during pharyngeal cartilage development. Besides, *mynn* deficiency-induced cell apoptosis was ubiquitously detected in the whole embryo and occurred mostly in the eye and brain (Figure S5B), suggesting that *mynn* is broadly required for cell viability during embryo development.

It is well known that the tumor suppressor p53 plays a primary role in inducing apoptosis in many cell types, including chondrocytes (Ito et al., 2014; Komori, 2016; Ning et al., 2013; Vogelstein and Kinzler, 1992). To

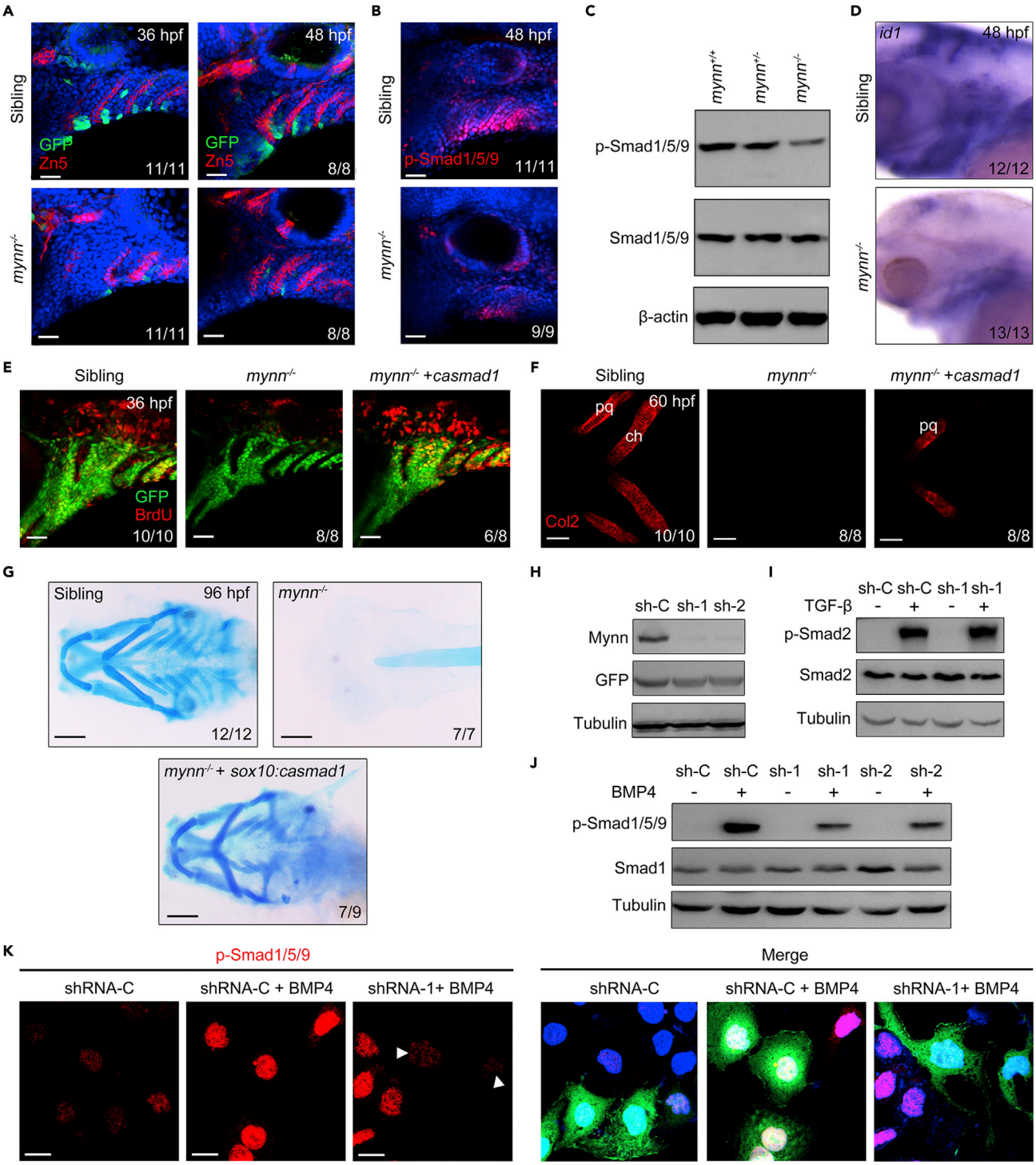

Figure 5. Mynn negatively regulates BMP signaling

(A) Expression of dGFP reporter in the pharyngeal region. *Mynn*$^{-/-}$ mutants and their siblings in *Tg(BRE:dGFP)* background were stained with the indicated antibodies. Nuclei were counterstained with DAPI (blue). Lateral views, anterior to the left. Scale bars, 20 μm.

(B and C) Expression of p-Smad1/5/9 was dramatically reduced in *mynn*$^{-/-}$ mutants. *mynn*$^{-/-}$ embryos and their siblings were harvested at 48 hpf, and then stained with anti-p-Smad1/5/9 antibodies (B). Scale bars, 20 μm. The levels of p-Smad1/5/9 in cell lysis of head region were further analyzed by Western blots (C).

(D) Expression levels of BMP target gene *id1* were detected by *in situ* hybridization. Embryos were lateral views with anterior to the left.

Figure 5. *Continued*

(E) Reactivation of BMP signaling can restore the proliferation of CNCCs in *mynn* mutant embryos. *mynn*$^{-/-}$ embryos in *Tg(fli1:EGFP)* background were injected with or without 10 pg mRNA encoding constitutively active Smad1 protein (caSmad1) at the one-cell stage, and incubated with BrdU at 34 hpf, then harvested at 36 hpf for staining with anti-BrdU (red) and anti-GFP (green) antibodies. Scale bars, 20 μm.

(F) Reactivation of BMP signaling can partially restore the differentiation of CNCCs in *mynn*$^{-/-}$ mutants. *mynn*$^{-/-}$ embryos were injected with or without 10 pg *casmad1* mRNA at the one-cell stage and then immunostained with anti-Col2 antibody at 72 hpf. pq, palatoquadrate; ch, ceratohyal. Scale bars, 20 μm.

(G) Alcian blue staining on embryos from different genotypes. Note that the missing cartilages in *mynn*$^{-/-}$ mutants could be rescued by specific overexpression of *casmad1* in *sox10*$^{+}$ NCCs. Scale bars, 200 μm.

(H) The effectiveness of Mynn shRNAs. HEK293T cells were transfected with the indicated shRNA plasmids and harvested 48 h after transfection for Western blot analyses.

(I and J) HEK293 cells transfected with indicated shRNA plasmids were treated with TGF-β1 (5 ng/mL) for 2 h (I) or BMP4 (20 ng/mL) for 4 h (J), and then collected for Western blots with the indicated antibodies.

(K) Hep3B cells transfected with plasmids expressing indicated shRNAs and GFP proteins were treated with or without BMP4 for 4 h. The expression levels of p-Smad1/5/9 were determined with immunostaining. As indicated with white arrowheads, the expression of p-Smad1/5/9 was obviously decreased in the cells expressing Mynn shRNAs. Scale bars, 20 μm.

identify the mechanism underlying the effect of *mynn* deficiency on the apoptosis of chondrogenic cells, we performed WISH experiments to examine whether p53 signaling was elevated in *mynn*$^{-/-}$ mutants. A drastic increase of *p53* expression was observed in *mynn*$^{-/-}$ embryos at 48 hpf (Figure 4C). Interestingly, the elevated *p53* transcripts were mainly restricted to the eye, brain, and pharyngeal region. Furthermore, when compared with control groups, *gadd45αa* expression—a conventional downstream gene of *p53*—was concomitantly increased in *mynn*-depleted embryos (Figure 4C). The upregulation of these pro-apoptotic genes was further validated by quantitative RT-PCR analysis (Figure 4D). These data imply that the p53 apoptotic pathway may be involved in *mynn* deficiency-induced apoptosis.

Finally, we tested whether *p53* inactivation could rescue the cell survival defects observed in *mynn*$^{-/-}$ mutants. To verify this, we generated double mutants by crossing *mynn*$^{+/-}$ fish with *p53*$^{-/-}$ mutants. In the resulting *mynn*$^{-/-}$;*p53*$^{-/-}$ embryos, there was a clear decrease in apoptotic cells in the pharyngeal region. However, these apoptotic cells were not completely eliminated (Figures 4E–4G). Furthermore, depletion of *p53* could not recover the loss of pharyngeal cartilages in *mynn*$^{-/-}$ mutants, indicating *mynn* is doing more than just cell survival, consistent with its crucial role in the proliferation and differentiation of CNCCs. Taken together, these results strongly suggest that the absence of *mynn* induces chondrogenic cell apoptosis. Moreover, this effect is partially caused by activation of the p53 pathway.

mynn inactivation attenuates BMP signaling

Our previous study found that the inhibition of BMP signaling resulted in poor proliferation, impaired differentiation, and unsustainable survival of chondrogenic progenitors (Ning et al., 2013). Since *mynn*$^{-/-}$ mutants phenocopied most of the abnormal behaviors of chondrogenic progenitors induced by BMP signaling deficiency, we next asked whether *mynn* functions in regulating BMP signaling during pharyngeal cartilage development. To characterize the temporal and spatial differences of BMP signal activity between siblings and *mynn*$^{-/-}$ mutants, we used a BMP signal reporter transgenic line *BRE:dGFP*. This transgenic line expressed a destabilized form of GFP (dGFP) driven by the BMP response element (BRE) derived from the mouse promoter *Id1* (Collery and Link, 2011). When compared with control animals, *mynn*$^{-/-}$ mutants showed much lower levels of GFP fluorescence intensity in the ventral arch domains at 36 and 48 hpf (Figure 5A), suggesting a requirement of *mynn* in BMP signal maintenance in CNCCs.

We further examined the spatial distribution of phosphorylated Smad1/5/9 (p-Smad1/5/9)—intracellular effectors of BMP signaling—using immunostaining in *mynn*$^{-/-}$ mutants and their siblings. Consistent with previous reports (Alexander et al., 2011; Ning et al., 2013), in control embryos, a gradient of p-Smad1/5/9 expression was detected in the pharyngeal region. More specifically, high levels were observed ventrally, while low levels were observed dorsally (Figure 5B). In contrast, the phosphorylation of Smad proteins was seriously compromised in the absence of *mynn* (Figure 5B). Corroborating these findings, Western blotting also showed a marked reduction of p-Smad1/5/9 levels in the head tissues of *mynn*$^{-/-}$ mutants (Figure 5C). Moreover, the expression of *id1*—the classic target gene of BMP—was notably reduced in the pharyngeal arch skeletons of embryos lacking the *mynn* gene (Figure 5D). Taken together, these results indicate that *mynn* is indispensable for BMP signal activity in pharyngeal chondrogenic progenitors. Surprisingly, injection of *mynn* mRNA into wild-type embryos did not induce a ventralized phenotype usually produced by excessive BMP signaling (Figure S6A), suggesting that Mynn is not sufficient to activate BMP signaling, but rather maintains it.

We next want to know if an elevated BMP signal can rescue the cartilage defects in *mynn*$^{-/-}$ embryos. To test this, mRNA encoding a constitutively active Smad1 protein (caSmad1)—the phosphomimetic form of Smad1, in which the C-terminal SVS motif was mutated to an aspartic acid-valine-aspartic acid (DVD) sequence—was injected into *mynn*$^{-/-}$ embryos at the one-cell stage (Tsukamoto et al., 2014). To avoid possible effects on embryonic dorsoventral patterning, a small dose of *casmad1* mRNA (10 pg) was injected into each embryo. We found that such injection did not result in obvious ventralized phenotypes, but completely rescued the proliferation defect in *mynn*-defective CNCCs (Figures 5E and S6B). However, although overexpression of *casmad1* in *mynn*$^{-/-}$ mutants partially alleviated the impaired chondrogenic differentiation at 60 hpf (Figure 5F), it did not improve the defects in cartilage formation at 96 hpf. Meanwhile, the morphological malformations in *mynn*$^{-/-}$ mutants were not eliminated in the rescue experiments (Figure S6B). The inefficiency of such rescue experiments might be due to the much lower dose of *casmad1* mRNA injection and the degradation of injected mRNA at later stages. To overcome these drawbacks, *casmad1* was specifically overexpressed in NCCs of *mynn*$^{-/-}$ mutants using the *sox10* promoter. As shown in Figure 5G, the NCC-specific overexpressed *casmad1* almost perfectly restored the loss of pharyngeal cartilages in *mynn*$^{-/-}$ mutant embryos. Based on these observations, we proposed that Mynn regulates pharyngeal cartilage development via upholding BMP signaling. In addition, the morphological abnormalities except pericardial edema in *mynn*$^{-/-}$ mutant were eliminated by NCC-specific overexpression of *casmad1* (Figure S6C), suggesting the non-cell-autonomous role of *mynn* also depends on its function in maintaining BMP signal activity.

To next clarify whether Mynn has a role in maintaining BMP signaling in mammalian cells, we designed two DNA constructs expressing independent short hairpin RNAs (shRNAs, termed Mynn shRNA1 and Mynn shRNA2) that targeted human Mynn. Both constructs were able to effectively inhibit Mynn expression (Figure 5H). As shown in Figures 5I and 5J, depletion of Mynn in human embryonic kidney 293 (HEK293) cells had no effect on TGF-β1-induced Smad2 phosphorylation, however, inhibited the phosphorylation of Smad1/5/9 triggered by BMP4, a well-known growth factor that induces the nuclear translocation of Smad proteins (Derynck and Budi, 2019). These results imply a specific function of Mynn in BMP signal transduction. Furthermore, the nuclear accumulation of p-Smad1/5/9, which was induced by BMP4 ligands, was significantly inhibited in Mynn-depleted hepatocellular carcinoma Hep3B cells (Figure 5K), indicating an evolutionarily conserved function of Mynn in BMP/Smad signal regulation.

Mynn physically interacts with Smad protein

Mynn is a nuclear protein that functions either directly or indirectly to modulate gene expression (Alliel et al., 2000; Kelly and Daniel, 2006). Given this, we hypothesized that Mynn regulates BMP signaling by interacting with Smad proteins, which constitutively shuttle between the cytoplasm and nucleus (Derynck and Budi, 2019). To test this, Flag-tagged Mynn was coexpressed with Myc-tagged Smad1 in HEK293 cells. After, co-immunoprecipitation (co-IP) experiments were performed using an anti-Flag antibody. Results indicated that Smad1 was co-precipitated with Mynn (Figure 6A). Importantly, we also found that overexpressed Myc-Smad1 was able to interact with endogenous Mynn (Figure 6B).

In general, the phosphorylated Smad proteins migrate more slowly than un-phosphorylated ones. We noted that immunoblotting with anti-Myc antibody revealed two bands that corresponded to a phosphorylated and an un-phosphorylated form of Smad1 in proteins co-precipitated with Mynn, although there was only a single anti-Myc band in the input lysates (Figure 6A). These observations may imply that Mynn prefers to interact with the phosphorylated form of Smad1, resulting in an efficient enrichment of phosphorylated Smad1 in the immunoprecipitated proteins. To address this, the interaction between Mynn and Smad1 was further examined in live cells by a bimolecular fluorescence complementation (BiFC) assay as previously described (Wei et al., 2017). The N-terminal half of yellow fluorescent protein (YFP) was fused to Mynn (YN-Mynn) while the C-terminal half of YFP was fused to Smad1 (YC-Smad1). Immunofluorescence staining revealed that YN-Mynn was localized to the nucleus; comparatively, YC-Smad1 was mainly distributed in the cytoplasm (Figure 6C). Interestingly, the reconstituted YFP signal was specifically observed in the nuclei (Figure 6D). Given this, it is likely that Mynn associates with nuclear Smad1 proteins, most of which are phosphorylated. Consistent with this idea, the association between Mynn and Smad1 was enhanced in the presence of BMP4 (Figure 6E).

Smads are structurally similar proteins containing two conserved polypeptide segments, the N-terminal MH1 and carboxyl-terminal MH2 domains linked by a less conserved linker region (Feng and Derynck, 2005). To determine which domain of the Smad protein is responsible for binding with Mynn, various

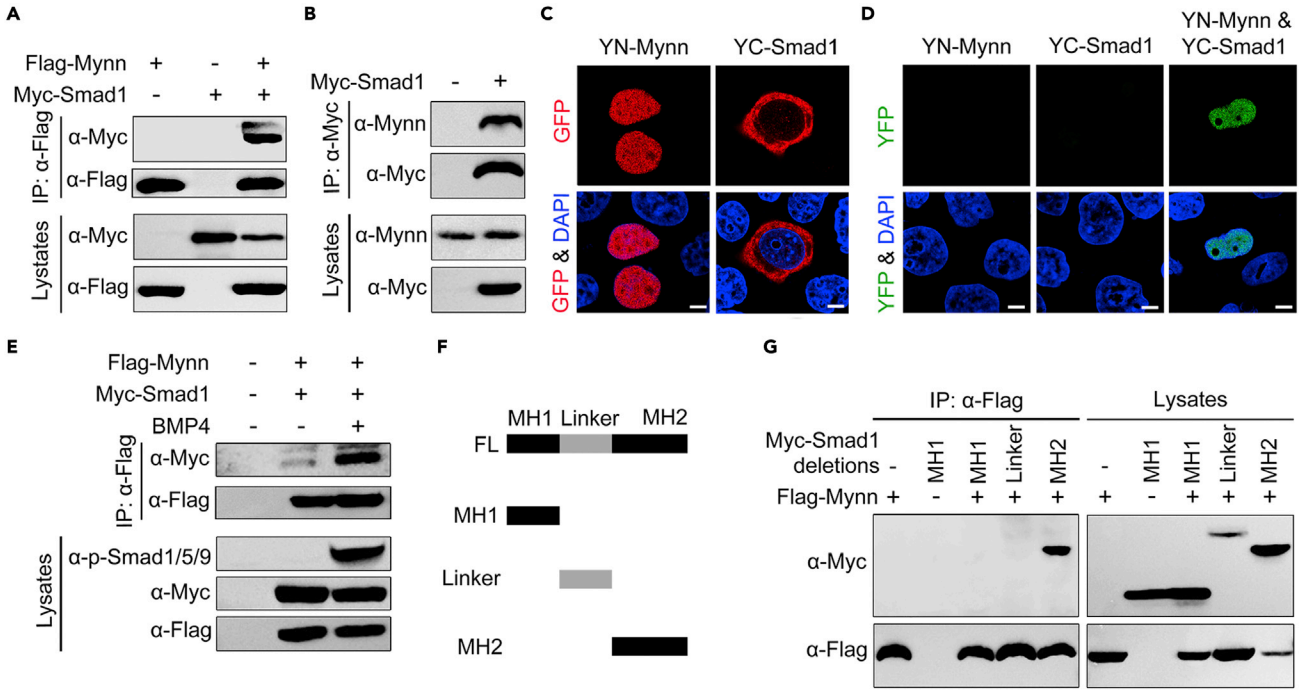

Figure 6. Mynn associates with Smad1

(A) Flag-tagged Mynn interacts with overexpressed Smad1. HEK293T cells were transfected with plasmids expressing Flag-Mynn and Myc-Smad1, and then harvested for immunoprecipitation with anti-Flag antibody.

(B) Overexpressed Smad1 interacts with endogenous Mynn. HEK293T cells transfected with Myc-tagged Smad1 were subjected to immunoprecipitation with anti-Myc antibody.

(C and D) Detection of Mynn-Smad1 interaction in living cells by BiFC assays. YN-Mynn and YC-Smad1 were transfected alone or simultaneously into HeLa cells. The expression of YN-Mynn or YC-Smad1 was detected by immunostaining with anti-GFP antibody (C). The reconstituted YFP fluorescence was detected by confocal microscopy at 488 nm (D). Scale bars: 10 μm.

(E) BMP4 treatment enhanced the interaction between Mynn and Smad1. HEK293T cells transfected with Myc-tagged Smad1 and Flag-tagged Mynn, and then treated with or without BMP4 for 4 h before being harvested for immunoprecipitation.

(F) Schematic representation of Smad1 truncations.

(G) Mynn binds to the MH2 domain of Smad1.

truncated mutants of Smad1 were constructed (Figure 6F). Domain mapping revealed that only the MH2 domain—neither the MH1 domain nor the linker region—interacted with Mynn (Figure 6G). Thus, these results indicate that Mynn binds to the MH2 domain of Smad1.

Mynn upholds BMP activity by competitively binding to the Smad protein with Ppm1a

The results presented above suggested that Mynn interacts with Smad proteins and maintains Smad phosphorylation in the nucleus. The next interesting question is how Mynn regulates the level of Smad phosphorylation. The receptor-regulated Smads undergo continuous nucleocytoplasmic shutting, and their export from the nucleus is controlled by a mechanism involving dephosphorylation (Lin et al., 2006; Xu et al., 2002). In particular, it has been suggested that Ppm1a, a serine/threonine phosphatase, binds to both the MH1 and MH2 domains of Smad1 and dephosphorylates Smad1 in the nucleus (Duan et al., 2006). Given that Mynn and Ppm1a each bind to the MH2 domain of Smad1, Mynn might compete with Ppm1a for this binding motif on Smad1.

This hypothesis prompted us to use co-IP experiments to investigate the effect of Mynn on the binding of Ppm1a to Smad1. Indeed, in HEK293 cells, we found that the presence of Mynn dramatically weakened the interaction between Ppm1a and Smad1 (Figure 7A). Next, we examined the effect of Mynn on Ppm1a-induced dephosphorylation of Smad1. Ectopic expression of ALK1 (Q233D), a constitutively active form of BMP type I receptor (caALK1), led to a dramatic elevation of Smad1 phosphorylation. This phosphorylation was almost abolished by coexpression of Ppm1a (Figure 7B). It is noteworthy that, in the presence of Mynn, the Ppm1a-induced elimination of Smad1 phosphorylation was obviously reduced (Figure 7B).

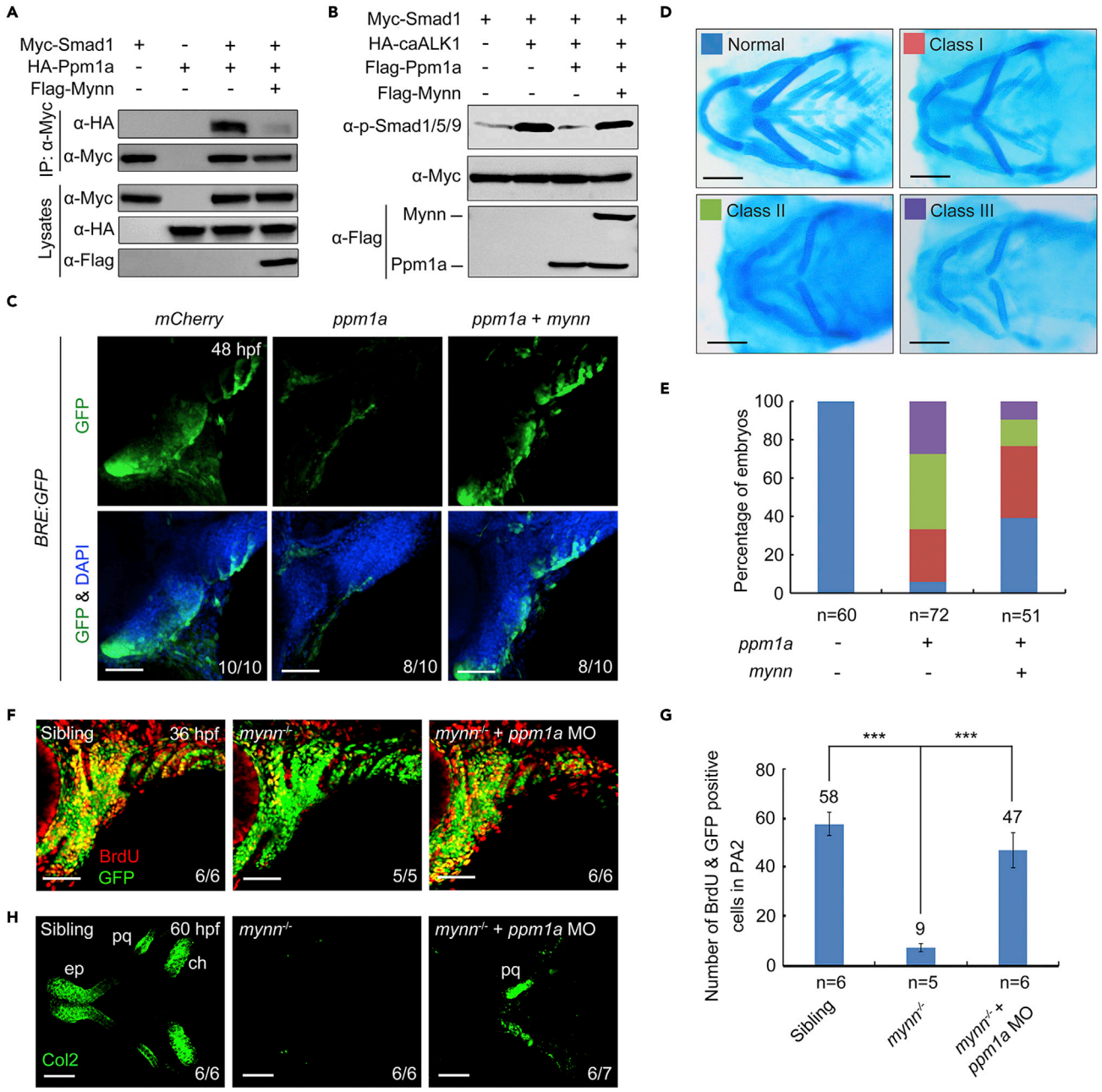

Figure 7. Mynn promotes BMP signaling through competing with Ppm1a for Smad binding

(A) Presence of Mynn attenuates the interaction of Ppm1a and Smad1. HEK293T cells were co-transfected with Myc-Smad1 and HA-Ppm1a together with or without Flag-Mynn, and then harvested for immunoprecipitation.

(B) Mynn weakens the Ppm1a-mediated dephosphorylation of p-Smad1/5/9. HEK293T cells were transfected with the indicated constructs. CaALK1 is a constitutively active form of BMP type 1 receptor ALK1 (Q233D). The expression levels of p-Smad1/5/9 and total Smad1 were detected by Western blots with appropriate antibodies.

(C) Overexpression of *mynn* can restore the decrease of BMP signal activity caused by excessive Ppm1a. *Tg(BRE:dGFP)* embryos were injected with indicated mRNAs at the one-cell stage and subjected to immunostaining for GFP (green) at 48 hpf. Scale bars, 50 μm. Injection dosages: *mCherry* mRNA, 400 pg; *ppm1a* mRNA, 400 pg; *mynn* mRNA, 300 pg.

(D and E) Ppm1a-induced pharyngeal cartilage defects were compromised by overexpression of *mynn*. Wild-type embryos were injected with 400 pg *ppm1a* mRNA together with or without 300 pg *mynn* mRNA at the one-cell stage, and stained at 96 hpf for cartilage with Alcian blue. Representative pictures of different classes of defects in pharyngeal cartilages were shown in (D). The percentage of embryos with different degrees of cartilage defects was calculated (E). Scale bars, 200 μm.

Figure 7. *Continued*

(F and G) Knockdown of *ppm1a* could restore the CNCC proliferation defects in *mynn*$^{-/-}$ mutants. *mynn*$^{-/-}$ mutant embryos were injected with 5 ng *ppm1a* MO at the one-cell stage and incorporated with BrdU at 34 hpf, and then harvested at 36 hpf for immunostaining with anti-BrdU (red) and anti-GFP (green) antibodies (F). Scale bars, 50 μm. The number of BrdU and GFP double positive cells in the second pharyngeal arch was calculated (G). Error bars indicate ±S.D. Student's *t*-test, ***, $p < 0.001$.

(H) The differentiation defects of CNCCs in *mynn* mutant embryos were partially recovered by *ppm1a* knockdown. *mynn*$^{-/-}$ embryos were injected with 5 ng *ppm1a* MO at the one-cell stage and harvested at 60 hpf for immunostaining with anti-Col2 (green) antibody. pq, palatoquadrate; ep, ethmoid plate; ch, ceratohyal. Scale bars, 50 μm.

To demonstrate the effect of Mynn on Ppm1a-mediated BMP signal suppression during pharyngeal skeleton formation, *Tg(BRE:dGFP)* embryos were injected with *ppm1a* mRNA together with or without *mynn* mRNA. It has been suggested that Ppm1a can also dephosphorylate Smad2/3 to inhibit Nodal signaling during zebrafish early embryogenesis (Lin et al., 2006). Indeed, a portion of embryos injected with *ppm1a* mRNA exhibited notochord defects, including discontinuous anterior notochord and thinner posterior notochord (Figures S7A and S7B), which are usually observed in Nodal-deficient mutants (Lin et al., 2006). However, overexpression of *mynn* in embryos-injected *ppm1a* mRNA could not obviously improve these morphological defects (Figures S7A and S7B), further confirming our finding that Mynn has a specific role in helping to maintain BMP but not TGF-β/Nodal signal activity. Importantly, in agreement with the crucial role of Ppm1a in dephosphorylation Smad1/5/9, ectopic expression of Ppm1a evidently decreased BMP signaling in the pharyngeal region and disrupted cartilage formation (Figures 7C–7E). Notably, both the reduction of BMP activity and the defects of pharyngeal cartilages in Ppm1a-overexpressed embryos were effectively relieved after Mynn coexpression (Figures 7C–7E).

To further explore the role of *mynn* in pharyngeal cartilage development, we hypothesized that suppression of *ppm1a* expression in *mynn*$^{-/-}$ mutants would rescue the CNCC proliferation and differentiation defects. To verify this, we designed a MO that could effectively block *ppm1a* translation (Figure S7C). We found that in *mynn*$^{-/-}$ mutant embryos injected with *ppm1a* MO, the proliferation ability of CNCCs was well recovered and the chondrogenic differentiation was partially rescued (Figures 7F–7H).

Based on the totality of these data, we present a model in which Mynn competes with Ppm1a for the MH2 domain on Smad proteins to uphold BMP signaling during cartilage formation. Mynn absence leads to more Ppm1a proteins associating with and subsequently dephosphorylating Smads. This then turns off BMP signaling, ultimately, resulting in impaired formation of pharyngeal cartilages.

DISCUSSION

Members of the BTB/POZ-ZF family are involved in a multitude of developmental events in invertebrates and vertebrates (Adhikary et al., 2003; Barna et al., 2000; Giniger et al., 1994; Pengue et al., 1994; Piazza et al., 2004; Xiong and Montell, 1993). Mynn is a novel member of the BTB/POZ-ZF family and is expressed in various tissues in human and mice, including cerebellum, testis, ovary, placenta, heart, brain, liver, and muscle (Alliel et al., 2000). Recently, Mynn has been suggested to be involved in tumorigenesis (Polat et al., 2019; Ramakrishna et al., 2010). However, its physiological functions during embryonic development remain poorly understood.

In this study, we identified a zebrafish line in which the *mynn* locus was interrupted by a Tol2 transposon. Zebrafish *mynn* transcripts are maternally deposited and ubiquitously expressed during the gastrulation stage and segmentation period. From 24 hpf, *mynn* expression is mainly restricted to the central nervous system, muscles, and pharyngeal arches, suggesting a conserved expression pattern across vertebrate species. *mynn* mutant embryos show a normal external morphology at early developmental stages, but display a variety of abnormalities at later stages, such as smaller head and eyes, coarse and rough skin, curved tail, and missing pharyngeal skeletons. However, because all of *mynn* zygotic mutants died at approximately 120 hpf, we were unable to generate maternal-zygotic *mynn* mutants. The phenotype we observed in *mynn* mutants was only an indication of loss-of-function effect of zygotic *mynn*. As such, it is impossible to ignore the possibility that *mynn* has unknown functions at early stages of embryogenesis, which may be masked by the persistence of maternal transcripts and proteins.

Because the head skeletons were almost completely missing in *mynn* mutants, we focused on the role of *mynn* in the development of pharyngeal cartilages. Our study reveals an essential role for *mynn* in CNCC proliferation, differentiation, and survival. Although expressed in multiple head tissues, *mynn* plays

a particularly important and cell-autonomous role during pharyngeal cartilage development. This was evidenced when re-supplying Mynn to NCCs restored cartilage formation in *mynn* mutants. Interestingly, such NCC-specific expression of *mynn* in the mutants also relieved most morphological defects, including smaller heads and eyes, rough skin, and curved tails. Because the cranial and trunk NCCs and their derived mesenchymal cells are required to support the growth and development of various kinds of tissues, such as thymic epithelium, pharyngeal arch artery, and hematopoietic stem cells (Blackburn and Manley, 2004; Damm and Clements, 2017; Ohnemus et al., 2002), it is reasonable to hypothesize that NCC-expressed *mynn* also has a non-cell-autonomous function of during embryogenesis.

Embryos depleted for *mynn* exhibited similar abnormal behaviors of chondrogenic progenitors induced by deficient BMP signaling as we have previously reported (Ning et al., 2013). Indeed, loss of Mynn in zebrafish embryos and mammalian cells resulted in a dramatic reduction in BMP signal activity, indicating a conserved function of Mynn in regulating BMP signaling. Moreover, NCC-specific overexpressed *casmad1* not only restored the loss of pharyngeal cartilages, but also recovered most morphological abnormalities in $mynn^{-/-}$ mutant, suggesting both the cell-autonomous and non-cell-autonomous roles of *mynn* depend on its function in maintaining BMP signal activity. A number of studies have indicated that single nucleotide polymorphisms in Mynn are associated with both the development and progression in colorectal, ovarian, and bladder cancers (Do et al., 2015; Houlston et al., 2010; Lubbe et al., 2012; Polat et al., 2019; Song et al., 2018). Furthermore, alterations in BMP signaling have been implicated in the pathogenesis of several tumor types including prostate, colorectal, osteosarcomas, myelomas, and breast cancers (Blanco Calvo et al., 2009; Sagorny et al., 2012; Wang et al., 2019). Therefore, our findings also provide meaningful clues for exploring the function of Mynn in tumorigenesis.

It has been reported that BMP signaling is negatively regulated by a few phosphatases, including Smad phosphatase Ppm1a (Duan et al., 2006; Lin et al., 2006). In this study, we find that Mynn physically interacts with Smad1 in the nucleus. The Mynn and Ppm1a proteins compete for binding with the Smad proteins, thus balancing BMP signaling for proper cartilage formation. Interestingly, previous work has also suggested that the BTB/POZ zinc finger family member Kaiso directly represses canonical Wnt signaling by associating with LEF/TCF proteins (Park et al., 2005). Given this, BTB/POZ zinc finger proteins are tightly linked to specific intracellular signaling pathways. However, overexpression of *casmad1* in $mynn^{-/-}$ mutants by mRNA injection or using *sox10* promoter could not rescue the pericardial defect. One possible explanation for this is that, in addition to regulating BMP signaling, Mynn may also play a role as a transcription factor to control gene expression during embryo development.

In summary, our data support the idea that Mynn is crucial for pharyngeal cartilage development by maintaining an adequate level of canonical BMP pathway activity. Mynn relieves Ppm1a-mediated dephosphorylation through competitive binding to Smad proteins. Therefore, our study provides new insight into the regulatory interactions between Mynn and BMP signaling during vertebrate development.

Limitations of the study

This study mainly explored the role for Mynn in balancing BMP signal activity through competitive binding to Smad proteins with Ppm1a during pharyngeal cartilage development. Mynn is a transcription factor that belongs to the BTB/POZ-ZF family, and *mynn* mutants exhibit various developmental defects in multiple tissues and organs. Future work is necessary to determine whether Mynn has a more widespread effect by acting as a transcription factor during embryo development as well, potentially independent of BMP signaling.

STAR★METHODS

Detailed methods are provided in the online version of this paper and include the following:

- KEY RESOURCES TABLE
- RESOURCE AVAILABILITY
  - Lead contact
  - Materials availability
  - Data and code availability
- EXPERIMENTAL MODEL AND SUBJECT DETAILS
  - Zebrafish strains

- Cell lines
- Generation of zebrafish line T054

- METHOD DETAILS
  - Morpholino, mRNA and microinjection
  - Alcian blue staining
  - 5′-RACE, genotyping, and quantitative real-time PCR
  - Whole-mount *in* situ hybridization and immunostaining
  - Proliferation and apoptosis analyses
  - Immunoprecipitation and Western blotting
  - RNA interference
  - BiFC assay
  - Quantification and statistical analysis

SUPPLEMENTAL INFORMATION

Supplemental information can be found online at https://doi.org/10.1016/j.isci.2022.104495.

ACKNOWLEDGMENTS

This work was supported by grants from the National Natural Science Foundation of China, Beijing, China (32025014, 81921006, and 30900843), the National Key Research and Development Program of China (2020YFA0804000 and 2018YFA0800200), CAMS Initiative for Innovative Medicine (2016-I2M-1-008), Public Service Development and Reform pilot Project of Beijing Medical Research Institute (BMR2019-11), and the Pediatric Medical Coordinated Development Center of Beijing Hospitals Authority (XTZD20180402).

AUTHOR CONTRIBUTIONS

S.Y. designed, performed the majority of experiments, analyzed the data, and wrote the original draft. G.N. performed the majority of experiments in the revised paper and involved in data generation and interpretation. Y.H performed *in situ* hybridization experiments and raised the zebrafish lines. Critical reagents were provided by Y.C. and J.X. J.W. and T. Z. discussed the results and editing the manuscript. Q.W. designed experiments, interpreted data, and revised the manuscript. All authors contributed to manuscript editing and review.

DECLARATION OF INTERESTS

The authors declare no competing interests.

Received: May 8, 2021
Revised: April 7, 2022
Accepted: May 23, 2022
Published: June 17, 2022

REFERENCES

Adhikary, S., Peukert, K., Karsunky, H., Beuger, V., Lutz, W., Elsässer, H.P., Möröy, T., and Eilers, M. (2003). Miz1 is required for early embryonic development during gastrulation. Mol. Cell Biol. *23*, 7648–7657. https://doi.org/10.1128/mcb.23.21.7648-7657.2003.

Alexander, C., Zuniga, E., Blitz, I.L., Wada, N., Le Pabic, P., Javidan, Y., Zhang, T., Cho, K.W., Crump, J.G., and Schilling, T.F. (2011). Combinatorial roles for BMPs and Endothelin 1 in patterning the dorsal-ventral axis of the craniofacial skeleton. Development *138*, 5135–5146. https://doi.org/10.1242/dev.067801.

Alliel, P.M., Seddiqi, N., Goudou, D., Cifuentes-Diaz, C., Romero, N., Velasco, E., Rieger, F., and Périn, J.P. (2000). Myoneurin, a novel member of the BTB/POZ-zinc finger family highly expressed in human muscle. Biochem. Biophys. Res. Commun. *273*, 385–391. https://doi.org/10.1006/bbrc.2000.2862.

Bardwell, V.J., and Treisman, R. (1994). The POZ domain: a conserved protein-protein interaction motif. Genes Dev. *8*, 1664–1677. https://doi.org/10.1101/gad.8.14.1664.

Barna, M., Hawe, N., Niswander, L., and Pandolfi, P.P. (2000). Plzf regulates limb and axial skeletal patterning. Nat. Genet. *25*, 166–172. https://doi.org/10.1038/76014.

Berghmans, S., Murphey, R.D., Wienholds, E., Neuberg, D., Kutok, J.L., Fletcher, C.D., Morris, J.P., Liu, T.X., Schulte-Merker, S., Kanki, J.P., et al. (2005). tp53 mutant zebrafish develop malignant peripheral nerve sheath tumors. Proc. Natl. Acad. Sci. U S A *102*, 407–412. https://doi.org/10.1073/pnas.0406252102.

Blackburn, C.C., and Manley, N.R. (2004). Developing a new paradigm for thymus organogenesis. Nat. Rev. Immunol. *4*, 278–289. https://doi.org/10.1038/nri1331.

Blanco Calvo, M., Bolós Fernández, V., Medina Villaamil, V., Aparicio Gallego, G., Díaz Prado, S., and Grande Pulido, E. (2009). Biology of BMP signalling and cancer. Clin. Transl. Oncol. *11*, 126–137. https://doi.org/10.1007/s12094-009-0328-8.

Carney, T.J., Dutton, K.A., Greenhill, E., Delfino-Machin, M., Dufourcq, P., Blader, P., and Kelsh, R.N. (2006). A direct role for Sox10 in specification of neural crest-derived sensory neurons. Development *133*, 4619–4630. https://doi.org/10.1242/dev.02668.

Chauchereau, A., Mathieu, M., de Saintignon, J., Ferreira, R., Pritchard, L.L., Mishal, Z., Dejean, A., and Harel-Bellan, A. (2004). HDAC4 mediates transcriptional repression by the acute promyelocytic leukaemia-associated protein PLZF. Oncogene *23*, 8777–8784. https://doi.org/10.1038/sj.onc.1208128.

Chen, W.Y., Zeng, X., Carter, M.G., Morrell, C.N., Chiu Yen, R.W., Esteller, M., Watkins, D.N., Herman, J.G., Mankowski, J.L., and Baylin, S.B. (2003). Heterozygous disruption of Hic1 predisposes mice to a gender-dependent spectrum of malignant tumors. Nat. Genet. *33*, 197–202. https://doi.org/10.1038/ng1077.

Chen, Z., Brand, N.J., Chen, A., Chen, S.J., Tong, J.H., Wang, Z.Y., Waxman, S., and Zelent, A. (1993). Fusion between a novel Krüppel-like zinc finger gene and the retinoic acid receptor-alpha locus due to a variant t(11;17) translocation associated with acute promyelocytic leukaemia. EMBO J. *12*, 1161–1167. https://doi.org/10.1002/j.1460-2075.1993.tb05757.x.

Cifuentes-Diaz, C., Bitoun, M., Goudou, D., Seddiqi, N., Romero, N., Rieger, F., Perin, J.P., and Alliel, P.M. (2004). Neuromuscular expression of the BTB/POZ and zinc finger protein myo-neurin. Muscle Nerve *29*, 59–65. https://doi.org/10.1002/mus.10526.

Collery, R.F., and Link, B.A. (2011). Dynamic smad-mediated BMP signaling revealed through transgenic zebrafish. Dev. Dynam. *240*, 712–722. https://doi.org/10.1002/dvdy.22567.

Cordero, D.R., Brugmann, S., Chu, Y., Bajpai, R., Jame, M., and Helms, J.A. (2011). Cranial neural crest cells on the move: their roles in craniofacial development. Am. J. Med. Genet. *155*, 270–279. https://doi.org/10.1002/ajmg.a.33702.

Couly, G., Creuzet, S., Bennaceur, S., Vincent, C., and Le Douarin, N.M. (2002). Interactions between Hox-negative cephalic neural crest cells and the foregut endoderm in patterning the facial skeleton in the vertebrate head. Development *129*, 1061–1073. https://doi.org/10.1242/dev.129.4.1061.

Crump, J.G., Maves, L., Lawson, N.D., Weinstein, B.M., and Kimmel, C.B. (2004). An essential role for Fgfs in endodermal pouch formation influences later craniofacial skeletal patterning. Development *131*, 5703–5716. https://doi.org/10.1242/dev.01444.

Damm, E.W., and Clements, W.K. (2017). Pdgf signalling guides neural crest contribution to the haematopoietic stem cell specification niche. Nat. Cell Biol. *19*, 457–467. https://doi.org/10.1038/ncb3508.

David, N.B., Saint-Etienne, L., Tsang, M., Schilling, T.F., and Rosa, F.M. (2002). Requirement for endoderm and FGF3 in ventral head skeleton formation. Development *129*, 4457–4468. https://doi.org/10.1242/dev.129.19.4457.

Derynck, R., and Budi, E.H. (2019). Specificity, versatility, and control of TGF-beta family signaling. Sci. Signal. *12*, eaav5183. https://doi.org/10.1126/scisignal.aav5183.

Dhordain, P., Lin, R.J., Quief, S., Lantoine, D., Kerckaert, J.P., Evans, R.M., and Albagli, O. (1998). The LAZ3(BCL-6) oncoprotein recruits a SMRT/mSIN3A/histone deacetylase containing complex to mediate transcriptional repression. Nucleic Acids Res. *26*, 4645–4651. https://doi.org/10.1093/nar/26.20.4645.

Do, S.K., Yoo, S.S., Choi, Y.Y., Choi, J.E., Jeon, H.S., Lee, W.K., Lee, S.Y., Lee, J., Cha, S.I., Kim, C.H., and Park, J.Y. (2015). Replication of the results of genome-wide and candidate gene association studies on telomere length in a Korean population. Korean J. Intern. Med. *30*, 719–726. https://doi.org/10.3904/kjim.2015.30.5.719.

Donoghue, P.C., Graham, A., and Kelsh, R.N. (2008). The origin and evolution of the neural crest. Bioessays *30*, 530–541. https://doi.org/10.1002/bies.20767.

Duan, X., Liang, Y.Y., Feng, X.H., and Lin, X. (2006). Protein serine/threonine phosphatase PPM1A dephosphorylates Smad1 in the bone morphogenetic protein signaling pathway. J. Biol. Chem. *281*, 36526–36532. https://doi.org/10.1074/jbc.M605169200.

Feng, X.H., and Derynck, R. (2005). Specificity and versatility in tgf-beta signaling through Smads. Annu. Rev. Cell Dev. Biol. *21*, 659–693. https://doi.org/10.1146/annurev.cellbio.21.022404.142018.

Giniger, E., Tietje, K., Jan, L.Y., and Jan, Y.N. (1994). lola encodes a putative transcription factor required for axon growth and guidance in Drosophila. Development *120*, 1385–1398. https://doi.org/10.1242/dev.120.6.1385.

Hall, B.K., and Miyake, T. (1995). Divide, accumulate, differentiate: cell condensation in skeletal development revisited. Int. J. Dev. Biol. *39*, 881–893.

Hamerman, D. (1989). The biology of osteoarthritis. N. Engl. J. Med. *320*, 1322–1330. https://doi.org/10.1056/NEJM198905183202006.

Han, Y., Mu, Y., Li, X., Xu, P., Tong, J., Liu, Z., Ma, T., Zeng, G., Yang, S., Du, J., and Meng, A. (2011). Grhl2 deficiency impairs otic development and hearing ability in a zebrafish model of the progressive dominant hearing loss DFNA28. Hum. Mol. Genet. *20*, 3213–3226. https://doi.org/10.1093/hmg/ddr234.

Houlston, R.S., Cheadle, J., Dobbins, S.E., Tenesa, A., Jones, A.M., Howarth, K., Spain, S.L., Broderick, P., Domingo, E., Farrington, S., et al. (2010). Meta-analysis of three genome-wide association studies identifies susceptibility loci for colorectal cancer at 1q41, 3q26.2, 12q13.13 and 20q13.33. Nat. Genet. *42*, 973–977. https://doi.org/10.1038/ng.670.

Ito, K., Maruyama, Z., Sakai, A., Izumi, S., Moriishi, T., Yoshida, C.A., Miyazaki, T., Komori, H., Takada, K., Kawaguchi, H., et al. (2014). Overexpression of Cdk6 and Ccnd1 in chondrocytes inhibited chondrocyte maturation and caused p53-dependent apoptosis without enhancing proliferation. Oncogene *33*, 1862–1871. https://doi.org/10.1038/onc.2013.130.

Kanzler, B., Foreman, R.K., Labosky, P.A., and Mallo, M. (2000). BMP signaling is essential for development of skeletogenic and neurogenic cranial neural crest. Development *127*, 1095–1104. https://doi.org/10.1242/dev.127.5.1095.

Kelly, K.F., and Daniel, J.M. (2006). POZ for effect–POZ-ZF transcription factors in cancer and development. Trends Cell Biol. *16*, 578–587. https://doi.org/10.1016/j.tcb.2006.09.003.

Kim, S.W., Park, J.I., Spring, C.M., Sater, A.K., Ji, H., Otchere, A.A., Daniel, J.M., and McCrea, P.D. (2004). Non-canonical Wnt signals are modulated by the Kaiso transcriptional repressor and p120-catenin. Nat. Cell Biol. *6*, 1212–1220. https://doi.org/10.1038/ncb1191.

Kimmel, C.B., Ballard, W.W., Kimmel, S.R., Ullmann, B., and Schilling, T.F. (1995). Stages of embryonic development of the zebrafish. Dev. Dynam. *203*, 253–310. https://doi.org/10.1002/aja.1002030302.

Knight, R.D., and Schilling, T.F. (2006). Cranial neural crest and development of the head skeleton. Adv. Exp. Med. Biol. *589*, 120–133. https://doi.org/10.1007/978-0-387-46954-6_7.

Kojima, S., Hatano, M., Okada, S., Fukuda, T., Toyama, Y., Yuasa, S., Ito, H., and Tokuhisa, T. (2001). Testicular germ cell apoptosis in Bcl6-deficient mice. Development *128*, 57–65. https://doi.org/10.1242/dev.128.1.57.

Komori, T. (2016). Cell death in chondrocytes, osteoblasts, and osteocytes. Int. J. Mol. Sci. *17*, 2045. https://doi.org/10.3390/ijms17122045.

LaBonne, C., and Bronner-Fraser, M. (1999). Molecular mechanisms of neural crest formation. Annu. Rev. Cell Dev. Biol. *15*, 81–112. https://doi.org/10.1146/annurev.cellbio.15.1.81.

Laux, D.W., Febbo, J.A., and Roman, B.L. (2011). Dynamic analysis of BMP-responsive smad activity in live zebrafish embryos. Dev. Dynam. *240*, 682–694. https://doi.org/10.1002/dvdy.22558.

Lawson, N.D., and Weinstein, B.M. (2002). In vivo imaging of embryonic vascular development using transgenic zebrafish. Dev. Biol. *248*, 307–318. https://doi.org/10.1006/dbio.2002.0711.

Li, L.W., Mao, A.H., Wang, P., Ning, G.Z., Cao, Y., and Wang, Q. (2018). Endodermal pouch-expressed dmrt2b is important for pharyngeal cartilage formation. Biol Open *7*, bio035444. https://doi.org/10.1242/bio.035444.

Liem, K.F., Jr., Tremml, G., Roelink, H., and Jessell, T.M. (1995). Dorsal differentiation of neural plate cells induced by BMP-mediated signals from epidermal ectoderm. Cell *82*, 969–979. https://doi.org/10.1016/0092-8674(95)90276-7.

Lin, X., Duan, X., Liang, Y.Y., Su, Y., Wrighton, K.H., Long, J., Hu, M., Davis, C.M., Wang, J., Brunicardi, F.C., et al. (2006). PPM1A functions as a smad phosphatase to terminate TGFβ signaling. Cell *125*, 915–928. https://doi.org/10.1016/j.cell.2006.03.044.

Lubbe, S.J., Whiffin, N., Chandler, I., Broderick, P., and Houlston, R.S. (2012). Relationship between 16 susceptibility loci and colorectal cancer phenotype in 3146 patients. Carcinogenesis *33*, 108–112. https://doi.org/10.1093/carcin/bgr243.

McConnell, M.J., Chevallier, N., Berkofsky-Fessler, W., Giltnane, J.M., Malani, R.B., Staudt, L.M., and Licht, J.D. (2003). Growth suppression

by acute promyelocytic leukemia-associated protein PLZF is mediated by repression of c-myc expression. Mol. Cell Biol. *23*, 9375–9388. https://doi.org/10.1128/mcb.23.24.9375-9388.2003.

McGurk, P.D., Lovely, C.B., and Eberhart, J.K. (2014). Analyzing craniofacial morphogenesis in zebrafish using 4D confocal microscopy. JoVEe51190. https://doi.org/10.3791/51190.

Nie, X., Luukko, K., and Kettunen, P. (2006). BMP signalling in craniofacial development. Int. J. Dev. Biol. *50*, 511–521. https://doi.org/10.1387/ijdb.052101xn.

Ning, G., Liu, X., Dai, M., Meng, A., and Wang, Q. (2013). MicroRNA-92a upholds Bmp signaling by targeting noggin3 during pharyngeal cartilage formation. Dev. Cell *24*, 283–295. https://doi.org/10.1016/j.devcel.2012.12.016.

Ohnemus, S., Kanzler, B., Jerome-Majewska, L.A., Papaioannou, V.E., Boehm, T., and Mallo, M. (2002). Aortic arch and pharyngeal phenotype in the absence of BMP-dependent neural crest in the mouse. Mech. Dev. *119*, 127–135. https://doi.org/10.1016/s0925-4773(02)00345-3.

Park, J.I., Kim, S.W., Lyons, J.P., Ji, H., Nguyen, T.T., Cho, K., Barton, M.C., Deroo, T., Vleminckx, K., Moon, R.T., and McCrea, P.D. (2005). Kaiso/p120-Catenin and TCF/β-Catenin complexes coordinately regulate canonical Wnt gene targets. Dev. Cell *8*, 843–854. https://doi.org/10.1016/j.devcel.2005.04.010.

Pengue, G., Calabró, V., Bartoli, P.C., Pagliuca, A., and Lania, L. (1994). Repression of transcriptional activity at a distance by the evolutionary conserved KRAB domain present in a subfamily of zinc finger proteins. Nucleic Acids Res. *22*, 2908–2914. https://doi.org/10.1093/nar/22.15.2908.

Piazza, F., Costoya, J.A., Merghoub, T., Hobbs, R.M., and Pandolfi, P.P. (2004). Disruption of PLZP in mice leads to increased T-lymphocyte proliferation, cytokine production, and altered hematopoietic stem cell homeostasis. Mol. Cell Biol. *24*, 10456–10469. https://doi.org/10.1128/mcb.24.23.10456-10469.2004.

Polat, F., Yilmaz, M., and Budak Diler, S. (2019). The association of MYNN and TERC gene polymorphisms and bladder cancer in a Turkish population. Urol. J. *16*, 50–55. https://doi.org/10.22037/uj.v0i0.4083.

Ramakrishna, M., Williams, L.H., Boyle, S.E., Bearfoot, J.L., Sridhar, A., Speed, T.P., Gorringe, K.L., and Campbell, I.G. (2010). Identification of candidate growth promoting genes in ovarian cancer through integrated copy number and expression analysis. PLoS One *5*, e9983. https://doi.org/10.1371/journal.pone.0009983.

Ruhin, B., Creuzet, S., Vincent, C., Benouaiche, L., Le Douarin, N.M., and Couly, G. (2003). Patterning of the hyoid cartilage depends upon signals arising from the ventral foregut endoderm. Dev. Dynam. *228*, 239–246. https://doi.org/10.1002/dvdy.10380.

Sagorny, K., Chapellier, M., Laperrousaz, B., and Maguer-Satta, V. (2012). [BMP and cancer: the Yin and Yang of stem cells]. Med. Sci. *28*, 416–422. https://doi.org/10.1051/medsci/2012284020.

Schneider, C.A., Rasband, W.S., and Eliceiri, K.W. (2012). NIH Image to ImageJ: 25 years of image analysis. Nat. Methods *9*, 671–675. https://doi.org/10.1038/nmeth.2089.

Schwend, T., and Ahlgren, S.C. (2009). Zebrafish con/disp1 reveals multiple spatiotemporal requirements for Hedgehog-signaling in craniofacial development. BMC Dev. Biol. *9*, 59. https://doi.org/10.1186/1471-213X-9-59.

Song, N., Kim, K., Shin, A., Park, J.W., Chang, H.J., Shi, J., Cai, Q., Kim, D.Y., Zheng, W., and Oh, J.H. (2018). Colorectal cancer susceptibility loci and influence on survival. Genes Chromosomes Cancer *57*, 630–637. https://doi.org/10.1002/gcc.22674.

Trainor, P., and Nieto, M.A. (2003). Jawsfest: new perspectives on neural crest lineages and morphogenesis. Development *130*, 5059–5063. https://doi.org/10.1242/dev.00768.

Tribulo, C., Aybar, M.J., Nguyen, V.H., Mullins, M.C., and Mayor, R. (2003). Regulation of Msx genes by a Bmp gradient is essential for neural crest specification. Development *130*, 6441–6452. https://doi.org/10.1242/dev.00878.

Tsukamoto, S., Mizuta, T., Fujimoto, M., Ohte, S., Osawa, K., Miyamoto, A., Yoneyama, K., Murata, E., Machiya, A., Jimi, E., et al. (2014). Smad9 is a new type of transcriptional regulator in bone morphogenetic protein signaling. Sci. Rep. *4*, 7596. https://doi.org/10.1038/srep07596.

Vogelstein, B., and Kinzler, K.W. (1992). p53 function and dysfunction. Cell *70*, 523–526. https://doi.org/10.1016/0092-8674(92)90421-8.

Wales, M.M., Biel, M.A., Deiry, W.E., Nelkin, B.D., Issa, J.P., Cavenee, W.K., Kuerbitz, S.J., and Baylin, S.B. (1995). p53 activates expression of HIC-1, a new candidate tumour suppressor gene on 17p13.3. Nat. Med. *1*, 570–577. https://doi.org/10.1038/nm0695-570.

Wang, Y., Zhu, P., Luo, J., Wang, J., Liu, Z., Wu, W., Du, Y., Ye, B., Wang, D., He, L., et al. (2019). LncRNA HAND2-AS1 promotes liver cancer stem cell self-renewal via BMP signaling. EMBO J. *38*, e101110. https://doi.org/10.15252/embj.2018101110.

Wei, S., Dai, M., Liu, Z., Ma, Y., Shang, H., Cao, Y., and Wang, Q. (2017). The guanine nucleotide exchange factor Net1 facilitates the specification of dorsal cell fates in zebrafish embryos by promoting maternal beta-catenin activation. Cell Res. *27*, 202–225. https://doi.org/10.1038/cr.2016.141.

Wilson, P.A., Lagna, G., Suzuki, A., and Hemmati-Brivanlou, A. (1997). Concentration-dependent patterning of the Xenopus ectoderm by BMP4 and its signal transducer Smad1. Development *124*, 3177–3184. https://doi.org/10.1242/dev.124.16.3177.

Xiong, W.C., and Montell, C. (1993). Tramtrack is a transcriptional repressor required for cell fate determination in the Drosophila eye. Genes Dev. *7*, 1085–1096. https://doi.org/10.1101/gad.7.6.1085.

Xu, L., Kang, Y., Col, S., and Massagué, J. (2002). Smad2 nucleocytoplasmic shuttling by nucleoporins CAN/Nup214 and Nup153 feeds TGFbeta signaling complexes in the cytoplasm and nucleus. Mol. Cell *10*, 271–282. https://doi.org/10.1016/s1097-2765(02)00586-5.

Yelick, P.C., and Schilling, T.F. (2002). Molecular dissection of craniofacial development using zebrafish. Crit. Rev. Oral Biol. Med. *13*, 308–322. https://doi.org/10.1177/154411130201300402.

Zhao, L., Zhao, X., Tian, T., Lu, Q., Skrbo-Larssen, N., Wu, D., Kuang, Z., Zheng, X., Han, Y., Yang, S., et al. (2008). Heart-specific isoform of tropomyosin4 is essential for heartbeat in zebrafish embryos. Cardiovasc. Res. *80*, 200–208. https://doi.org/10.1093/cvr/cvn177.

Zheng, X., Yang, S., Han, Y., Zhao, X., Zhao, L., Tian, T., Tong, J., Xu, P., Xiong, C., and Meng, A. (2012). Loss of zygotic NUP107 protein causes missing of pharyngeal skeleton and other tissue defects with impaired nuclear pore function in zebrafish embryos. J. Biol. Chem. *287*, 38254–38264. https://doi.org/10.1074/jbc.M112.408997.

STAR★METHODS

KEY RESOURCES TABLE

REAGENT or RESOURCE	SOURCE	IDENTIFIER
Antibodies		
Rabbit Phospho-Smad1 (Ser463/465)/Smad5 (Ser463/465)/Smad9 (Ser465/467) (D5B10) mAb	Cell Signaling Technology	Cat#13820
Rabbit Smad1 Antibody	Cell Signaling Technology	Cat# 9743
Mouse anti-Collagen type II	DSHB	Cat#II-II6B3
Mouse anti-Zn5	Zebrafish International Resource Center (ZIRC)	Cat#111605
Monoclonal Anti-BrdU Mouse	Sigma Aldrich	Cat#B-2531
Rabbit GFP Polyclonal Antibody	Thermo Fisher Scientific	Cat#A11122
Mouse Anti-FLAG® M2 Affinity Gel	Sigma Aldrich	Cat#A2220
Rabbit Anti-c-Myc Agarose Affinity Gel	Sigma Aldrich	Cat#A7470
Mouse DYKDDDDK-Tag(3B9) Antibody	Abmart	Cat#M20008M
Mouse Anti-Myc-tag mAb	MBL(Medical & Biological Laboratories)	Cat#M047-3
Mouse anti-Myoneurin (JB-17)	Santa Cruz Biotechnology	Cat# 101082
Sheep Anti-Digoxigenin-AP	Roche	Cat# 11093274910
Donkey anti-Rabbit, Alexa Fluor 488	Thermo Fisher Scientific	Cat# A-21206
Donkey anti-Mouse, Alexa Fluor 594	Thermo Fisher Scientific	Cat# A-21125
Donkey anti-Rabbit, Alexa Fluor 594	Thermo Fisher Scientific	Cat# A-21207
Donkey anti-Mouse, Alexa Fluor 647	Thermo Fisher Scientific	Cat# A-31571
Chemicals, peptides, and recombinant proteins		
4′,6-Diamidino-2-phenylindole dihydrochloride (DAPI)	Sigma Aldrich	Cat# 10236276001
Alcian Blue 8GX	Sigma Aldrich	Cat# 05500
5-bromo-2′-deoxyuridine (BrdU)	Sigma Aldrich	Cat# B5002
Methyl cellulose	Sigma Aldrich	Cat#M6385
Trypsin	AMRESCO	Cat#0458
Ethyl 3-aminobenzoate methanesulfonate salt (Tricaine)	Sigma Aldrich	Cat# A5040
N-Phenylthiourea (PTU)	Sigma Aldrich	Cat# P7629
Lipofectamine 2000	Thermo Fisher Scientific	Cat# 11668019
RNA Polymerase, T7	Roche	Cat#10881775001
RNA Polymerase, SP6	Roche	Cat#11487671001
DIG RNA Labeling Mix	Roche	Cat#11277073910
BMP4	R&D	Cat#314-BP-010
Critical commercial assays		
FirstChoice® RLM-RACE Kit	Thermo Fisher Scientific	Cat#AM1700
RNeasy Mini Kit	Qiagen	
In Situ Cell Death Detection Kit, TMR red	Roche	Cat#12156792910
ReverTra Ace	TOYOBO	Cat#TRT-101
Trelief™ SoSoo Cloning Kit	Tsingke Biotechnology	Cat#TSV-S2
TB Green® Premix Ex Taq™ II (Tli RNaseH Plus)	Takara	Cat# RR820A
mMESSAGE mMACHINE™ SP6	Thermo Fisher Scientific	Cat# AM1340
Experimental models: Cell lines		
HEK293T	ATCC	CRL-3216
HEK293	ATCC	CRL-1573

(*Continued on next page*)

Continued

REAGENT or RESOURCE	SOURCE	IDENTIFIER
Hep3B	ATCC	HB-8064
HeLa	ATCC	CCL-2
Experimental models: Organisms/strains		
Tg(fli1:EGFP)	(Lawson and Weinstein, 2002)	ZDB-TGCONSTRCT-070117-94
Tg(BRE:EGFP)	(Laux et al., 2011)	ZDB-FISH-150901-20390
tp53^{M214K}	(Berghmans et al., 2005)	ZDB-ALT-050428-2
mynn^{T054}	This paper	N/A
Oligonucleotides		
mynn-qPCR Forward: 5′-CAGTGTCCCCTCAACATCCC-3′	This paper	N/A
mynn-qPCR Reverse: 5′-GGAAGATCATGGAGGGCTCG-3′	This paper	N/A
gadd45αa-qPCR Forward:. 5′-CTTGCACTGCATTCTGGTCAC-3′	This paper	N/A
gadd45αa -qPCR Reverse: 5′-CTCATCGCTCTGGAAGGTTGC-3′	This paper	N/A
p53-qPCR Forward: 5′-CTTCTTCAGCTACATTACGACCTGAGGGGAGC-3′	This paper	N/A
p53-qPCR Reverse:. 5′-GCAGGCACCACATCACTTAACTCCAGACTG-3′	This paper	N/A
gapdh-qPCR Forward: 5′-AGGCCGGTGCTGAGTATGTC-3′	This paper	N/A
gapdh -qPCR Reverse:. 5′-TGCCTGCTTCACCACCTTCT-3′	This paper	N/A
genotyping-P1: 5′-CCGTCAAAGCAAAGCGATTTTAATCT-3′	This paper	N/A
genotyping-P2:5′-GGCTCTAAAGGCTCATAGTCATCTGG-3′	This paper	N/A
genotyping-P3: 5′-CCTAAGTACTTGTACTTTCACTTG-3′	This paper	N/A
mynn MO: 5′-CATGGCGTGTAGAGGAAAAACCTCA-3′	This paper	N/A
ppm1a MO: 5′-GGCTTATCCAGAAATGCACCCATGT-3′	This paper	N/A
control MO 5′-CCTCTTACCTCAGTTACAATTTATA-3′	Gene tools	
mynn shRNA NO1. 5′-GGAATGTGCTGGCCTCCTTTA-3′	This paper	N/A
mynn shRNA NO2. 5′-GCACACTGTTACAGTGAAACG-3′	This paper	N/A
Recombinant DNA		
TSG	(Han et al., 2011)	N/A
pCS2-flag-mynn	This paper	N/A
Pcdna3.0-6xmyc-smad1	This paper	
YN-mynn	This paper	N/A
YC-smad1	This paper	N/A
pCS2-myc-smad1-MH1	This paper	N/A
pCS2-myc-smad1-linker	This paper	N/A
pCS2-myc-smad1-MH2	This paper	N/A
pCS2-HA-ppm1a	This paper	N/A
pCS2-caAlk1	from Tsinghua University	N/A
pCS2-flag-ppm1a	(Duan et al., 2006)	N/A
pCS2-casmad1	from Tsinghua University	N/A
pSTG-*sox10:casmad1*-P2A-*mcherry*	This paper	N/A

(*Continued on next page*)

Continued

REAGENT or RESOURCE	SOURCE	IDENTIFIER
pSTG-*sox10:mynn*-P2A-*mcherry*	This paper	N/A
pCS2-Tol2	(Han et al., 2011)	
Software and algorithms		
ImageJ	(Schneider et al., 2012)	https://imagej.nih.gov/ij/
Microsoft Excel	Microsoft	N/A
GraphPad Prism 6	GraphPad Software	N/A
NIS-Elements	Nikon Instruments	N/A

RESOURCE AVAILABILITY

Lead contact

Further information and requests for resources and reagents should be directed to and will be fulfilled by the Lead Contact Qiang Wang (qiangwang@scut.edu.cn (Q.W.)).

Materials availability

Plasmids and animal models generated in this paper will be shared freely upon request to the lead contact.

Data and code availability

- Data: All data reported in this paper will be shared by the lead contact upon request.
- Code: This paper does not report original code.
- Any additional information required to reanalyze the data in this paper is available from the lead contact upon request.

EXPERIMENTAL MODEL AND SUBJECT DETAILS

Zebrafish strains

Zebrafish strains were maintained in stand laboratory conditions. Embryos were obtained from natural zebrafish matings, raised in Holtfreter's solution at 28.5°C, and staged by morphology as previously described (Kimmel et al., 1995). The following published strains were used in this study: *Tg(fli1:EGFP)* (Lawson and Weinstein, 2002); *Tg(BRE:EGFP)* (Laux et al., 2011) *and tp53* mutant (Berghmans et al., 2005). Live embryos or adults were anesthetized in fish water containing 0.4% tricaine (ethyl 3-aminobenzoate methanesulfonate salt; Sigma-Aldrich). Our work involving zebrafish embryo collection and analysis was carried out in accordance with and approved through the Animal Care Committee at the Institute of Zoology, Chinese Academy of Sciences (Permission Number: IOZ-13048).

Cell lines

HEK293 (CRL-1573, ATCC), HEK293T (CRL-3216, ATCC), Hep3B (HB-8064, ATCC) and HeLa cell lines (CCL-2, ATCC) were cultured in Dulbecco's modified Eagle's medium (DMEM, HyClone) supplemented with 10% fetal bovine serum (FBS, HyClone) and 1% penicillin-streptomycin (HyClone) at 37 °C in a humidified incubator with 5% CO2. Cell transfections were performed by using Lipofectamine 2000 (11668019, Invitrogen) according to the manufacturer's instructions.

Generation of zebrafish line T054

For transposon-mediated insertional mutagenesis, the transposon vector TSG was constructed as previously described (Han et al., 2011). 50 ng TSG plasmid and 100 pg *tol2* mRNA were injected into embryos at the one-cell stage. The injected founder (F0) embryos were raised to adulthood and outcrossed with wild-type fish, and their progeny (F1) were observed for GFP expression pattern under a fluorescence microscope. The GFP-positive embryos were grown up to establish Tol2 insertion mutant lines. Particularly, the T054 line was identified in such pilot experiments.

METHOD DETAILS

Morpholino, mRNA and microinjection

Capped mRNAs were synthesized *in vitro* for *mynn*, *casmad1*, *ppm1a*, and Tol2 from the corresponding linearized plasmids using the mMessage mMachine kit (Thermo Fisher Scientific, AM1340). *mynn* MO (5′-CATGGCGTGTAGAGGAAAAACCTCA-3′) and *ppm1a* MO (5′-GGCTTATCCAGAAATGCACCCATGT-3′) were designed to target the translational start regions, respectively. A non-targeting standard control MO (5′-CCTCTTACCTCAGTTACAATTTATA; Gene Tools) was used as a control for unspecific effects. Both mRNA and MO were injected into the yolk of one-cell stage embryos. In the rescue experiments, the recombinant plasmids *pSTG-sox10:mynn-P2A-mcherry* or *pSTG-sox10:casmad1-P2A-mcherry* and the *Tol2* mRNA were coinjected into fertilized eggs by microinjection.

Alcian blue staining

Embryos at 96 hpf were fixed in 4% paraformaldehyde overnight. Then embryos were washed in distilled water until the embryo was transparent. After staining with Alcian blue staining buffer (0.015% Alcian Blue, 80% ethanol, and 20% acetic acid) overnight at room temperature, the embryos were de-stained in ethanol of gradient concentrations. Next, the embryos were treated with 0.5% trypsin (0458, AMRESCO) in supersaturated borax at room temperature until the tissues were soft enough to dissect. The embryos were then transferred to 1% KOH and dehydrated with a graded series of glycerol solutions.

5′-RACE, genotyping, and quantitative real-time PCR

5′-RACE was performed using the FirstChoice® RLM-RACE Kit (Thermo Fisher Scientific, AM1700) according to the manufacturer's instructions.

For genotyping, embryos from T054 intercrosses were separated into three classes according to their fluorescence intensity at 24 hpf. Genomic DNA was extracted from single embryos for genotyping by PCR amplification with sequence-specific primers listed in the key resources table.

For quantitative real-time RT-PCR, total RNA of siblings and T054 embryos were extracted from a pool of 30 embryos at indicated stages by RNeasy Mini Kit (Qiagen, 74104). According to the manufacturer's instructions (TOYOBO, TRT-101), cDNAs were synthesized from 2 μg RNA using oligo-dT primer, and then quantitative real-time PCR was carried out with TB Green® Premix Ex Taq™ II (Takara, RR820A) in the Mx3000P real-time PCR system (Stratagene). Expression level of β-actin was analyzed as an internal control.

Whole-mount *in* situ hybridization and immunostaining

For whole mount *in situ* hybridization, Digoxigenin-UTP-labeled RNA probes were synthesized *in vitro* from linearized DNA templates using the RNA Polymerase T7/Sp6 system (Roche, Cat#10881775001/11487671001) according to the manufacturer's instructions. Whole-mount *in situ* hybridizations were performed following the standard procedure.

For immunostaining, embryos were fixed in 4% paraformaldehyde at 4°C for 24 h, and then dehydrated with methanol. The embryos were re-dehydrated through a series of washings with methanol in PBST. Then embryos were permeabilized with proteinase K (10 mg/mL) for 30 to 60 min and incubated in blocking buffer (2% BSA, 5% normal goat serum, 0.1% Tween-20 in PBS) for 1 h. Embryos were stained with the following affinity-purified antibodies: Rabbit anti-P-Smad1/5/9 (1:500; 18320, Cell Signaling Technology); Mouse anti-Collagen type II (1:100; II-116B3, DSHB); Zn5 (1:50; 111605, Zebrafish International Resource Center). Finally, the embryos were mounted in 1% low melting point agarose and imaged using a Nikon A1R+ confocal microscope.

Proliferation and apoptosis analyses

For all BrdU incorporation experiments, embryos were placed in 10 mM BrdU at specific stages for 20 min and then harvested. Incorporated BrdU and GFP were detected using anti-BrdU (1:1,000; B5002, Sigma) and rabbit anti-GFP antibodies (1:1,000, a gift from Dahua Chen Lab) by whole-mount immunostaining. TUNEL assays were performed using *In Situ* Cell Death Detection Kit, TMR red (12156792910, Roche) according to the manufacturer's instruction.

Immunoprecipitation and Western blotting

HEK293T cells were transiently transfected with indicated plasmids. 36 h after transfection, cells were harvested and lysed with TNE buffer (150 mM NaCl, 10 mM Tris-HCl (pH7.5), 2 mM EDTA, and 0.5% NonidetP-40) containing protease inhibitors. Immunoprecipitation and Western blots were performed according to standard protocols. For Western blots, affinity-purified anti-Flag (1:5000; M20008M, Abmart), anti-Myc (1:3000; M047-3, MBL), anti-Smad1 (1:1000; 9743, Cell Signaling Technology), anti-Mynn (1:200; SC-101082, Santa Cruz) and anti-P-Smad1/5/9 (1:500; 18320, Cell Signaling Technology) antibodies were used.

RNA interference

Two shRNAs against Mynn were designed (NO.1, 545-565, 5′-GGAATGTGCTGGCCTCCTTTA-3′, and NO.2, 1182-1202, 5′-GCACACTGTTACAGTGAAACG-3′). Oligonucleotides were chemically synthesized and subcloned into the U6/GFP/Neo shRNA vector by Gene Pharma (Shanghai, China).

BiFC assay

For the BiFC assay, Mynn was fused to the N-terminal half of YFP with restriction endonuclease cleavage sites EcoRI and SalI (YN-Mynn), while Smad1 was fused to the C-terminal half of YFP with restriction endonuclease cleavage sites BglII and ECoRI (YC-Smad1). YN-Mynn and YC-Smad1 were either individually or collectively transfected into HeLa cells. YFP fluorescence was visualized using a Nikon A1R+ confocal microscope at 48 h after transfection.

Quantification and statistical analysis

For GFP- and BrdU/TUNEL-positive cell counts, images were analyzed with Image J software. Statistical analysis was performed with Graph Pad Prism. All statistical values are displayed as mean ± standard deviation. Comparisons between experimental groups were performed using an unpaired two-tailed *t* test with unequal variance for parametric samples. Differences are considered significant at a $p < 0.05$ significance level and marked with ''*'', very significant at $p < 0.01$ and labeled with ''**'', and extremely significant at $p < 0.001$ and labeled with ''***''.